

## Dark etching regions under rolling contact fatigue: a review

S. Echeverri Restrepo<sup>a,b</sup>, S. W. Ooi<sup>c</sup>, P. Yan<sup>a</sup>, P. Andric<sup>a</sup>, R. H. Vegter<sup>a</sup>, and J. Lai<sup>a</sup>

<sup>a</sup>SKF Research & Technology Development (RTD), SKF B.V., Meidoornkade 14, 3992 AE, Houten, The Netherlands; <sup>b</sup>Department of Physics, King's College London, Strand, London WC2R 2LS, United Kingdom; <sup>c</sup>Ovako Group R&D, Maxwell Centre, University of Cambridge, JJ Thomson Avenue, Cambridge, CB3 0HE, United Kingdom

### ARTICLE HISTORY

Compiled April 7, 2021

### Abstract

Bearing performance depends on the ability of steel to cope with a large number of stress cycles. Long bearing lives are possible because the microstructure of bearing steel has excellent resistance to Rolling Contact Fatigue (RCF). Nevertheless, it is observed that the microstructure suffers changes in the region where the maximum Hertzian contact stress occurs. Here we give an overview of the present knowledge in the area of the formation of Dark Etching Regions (DERs) during RCF. Factors that influence the formation of DERs, various types of characterisation techniques, and the observations made in the literature are discussed. In addition, the applicability of several proposed simulation models of the formation of DERs is discussed.

## 1. Introduction

Rolling contact on the raceways of a bearing generates cyclic stresses that extend from surface to subsurface. The deviatoric stress, often referred to as the maximum shear stress or the Von Mises stress, is responsible for the onset and development of material damage in terms of plasticity and fatigue. When the accumulated damage exceeds a certain limit, the bearing will fail as a result of Rolling Contact Fatigue (RCF).

Under poor lubrication conditions, metal-to-metal contact at the asperity level may occur generating high deviatoric stresses on or near the surface, and cause surface fatigue. High surface stress can also be attributed to excessive surface traction, induced by sliding contact. Surface fatigue failure is often manifested as micro pitting. Other types of surface fatigue failures include wear, smearing, etc. [1,6].

When a bearing operates under good and clean lubrication conditions, the maximum deviatoric stress is located at a certain distance beneath the surface, as indicated in Figure 1 and the bearing may fail due to crack initiation and propagation from the subsurface. Subsurface initiated fatigue is characterised by isolated spall(s) on the raceway.

A functioning bearing is subject to external loads. If the external loads are high enough, the contact stresses between the rolling elements that pass over the raceway will reach the yield point of the material generating plastic flow and leaving residual

---

CONTACT S. Echeverri Restrepo. Email: [sebastianeecheverrir@gmail.com](mailto:sebastianeecheverrir@gmail.com)

CONTACT S. W. Ooi. Email: [steve.ooi@ovako.com](mailto:steve.ooi@ovako.com)

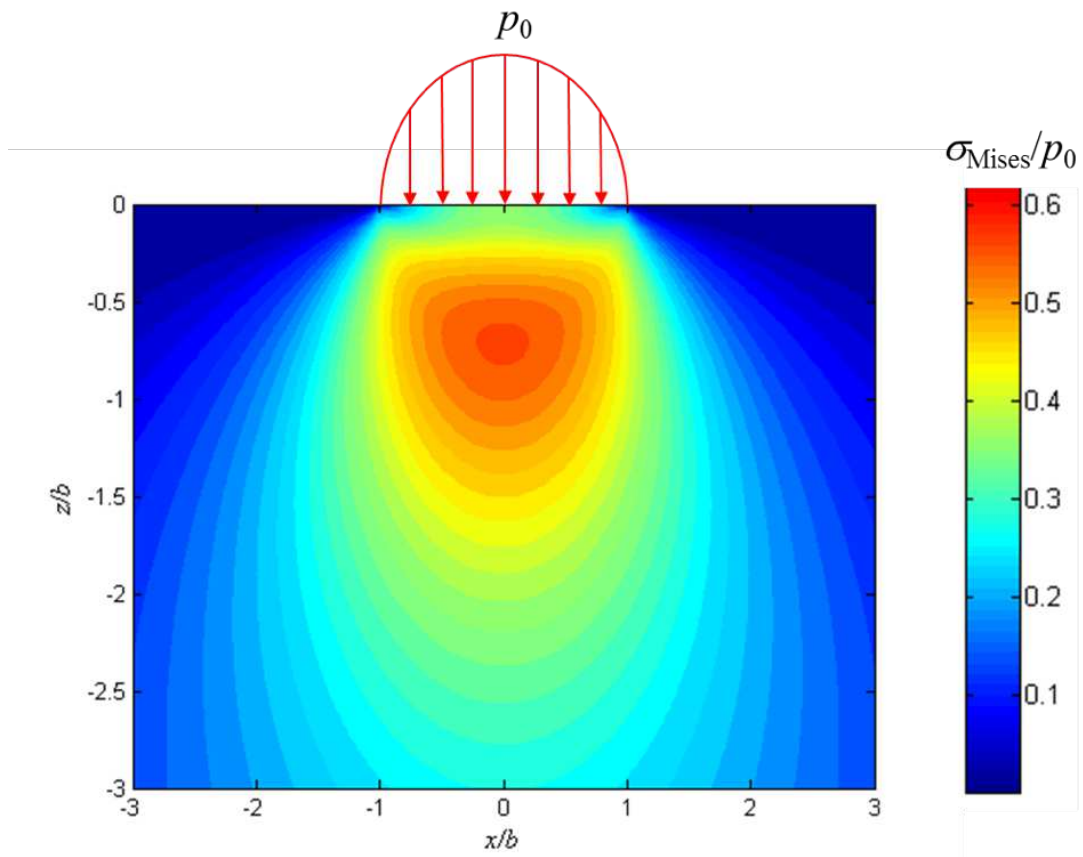


**Figure 1.** Distribution of subsurface von Mises stress resulting from Hertzian contact.

stresses. After a number of passes of the rolling elements, the combined applied and residual stresses might not reach the yield point, generating only elastic strain. This phenomenon is referred to as the “elastic shakedown”. The maximum stress that can be applied cyclically to the material for which the elastic shakedown can be reached is called the “elastic shakedown limit” [7-11].

Two types of fatigue damage may develop in the subsurface of a bearing. If the contact stress exceeds elastic shakedown limit, the subsurface material undergoes gradual but progressive plastic flow. As a result, large-scale microstructural alterations or decay of the steel microstructure will develop in the form of Dark Etching Regions (DERs), followed by the formation of White Etching Bands (WEBs) with a Low Angle of about 30° (LABs) and WEBs with a High Angle of about 80° (HABs), as shown in Figure 2. At a contact stress below the shakedown limit, localised damage can still develop from material defects or stress risers such as inclusions. This type of damage is typically characterised by the onset of the so-called “butterflies” with single or multiple cracks initiated from an inclusion or a pore, see Figure 3. The growth of the cracks is accompanied by the development of White Etching Matter (WEM) [12]. Subsurface cracks will grow initially in a co-planar manner and later kink or branch into multiple cracks towards the raceway, leading to spalling [13].

Relevant fatigue damage modes that may develop in the subsurface region of a rolling bearing are indicated by the fatigue damage map shown in Figure 4 where damage processes like DERs, LABs and HABs that occur at relatively high stresses above the elastic shakedown limit are classified as “global damage”, while butterflies and / or WECs that may develop from material imperfections are classified as “localised damage”. A schematic of the L10 curve, i.e. the calculated life with 10 % probability of failure, is also included in the fatigue damage map. The fatigue mechanisms that govern the material degradation occurring around or even before the calculated L10 will have a dominant effect on bearing fatigue life. The coloured bands indicate schematically the start of each specific mechanism. Although both modes of subsurface initiated fatigue are relevant for rolling bearings, the global damage is more frequently observed in ball bearings than in roller bearings. This is because the contact stresses in ball bearings in some applications can be relatively high and even exceed the shakedown limit of bearing steels. Furthermore, the stressed volume or volume at risk in ball bearings is relatively small and, statistically speaking, the number of stress raisers like inclusions, especially those big ones, is relatively small. In this case, both modes of fatigue damage may develop and, under certain circumstances, development of the global damage can prevail over that of localise damage. Roller bearings, however, are mostly operating at contact stresses below the shakedown limit, and thus the localised damage developed from stress raisers is the main failure mode as far as subsurface initiated fatigue is concerned. The diagram shown in Figure 4 was produced based on the information published in the literature. A similar representation can be found in [14,15], in which only global damage was included.

This article presents a review of the study of the global damage in bearing steels under rolling contact fatigue, focusing in particular on the formation and development of the Dark Etching Regions (DERs) from the perspectives of characterisation, mechanisms and modelling. In Section 2 we introduce some basic concepts. In Sections 3 and 4, we discuss the factors that affect the formation of DERs and the phenomena that are observed. In Sections 5 and 6 we introduce the mechanisms of formation and the different strategies that have been used to model them. We finally give a general discussion of what is available in the literature.

More general reviews on the topic of rolling contact fatigue can be found in [11] and

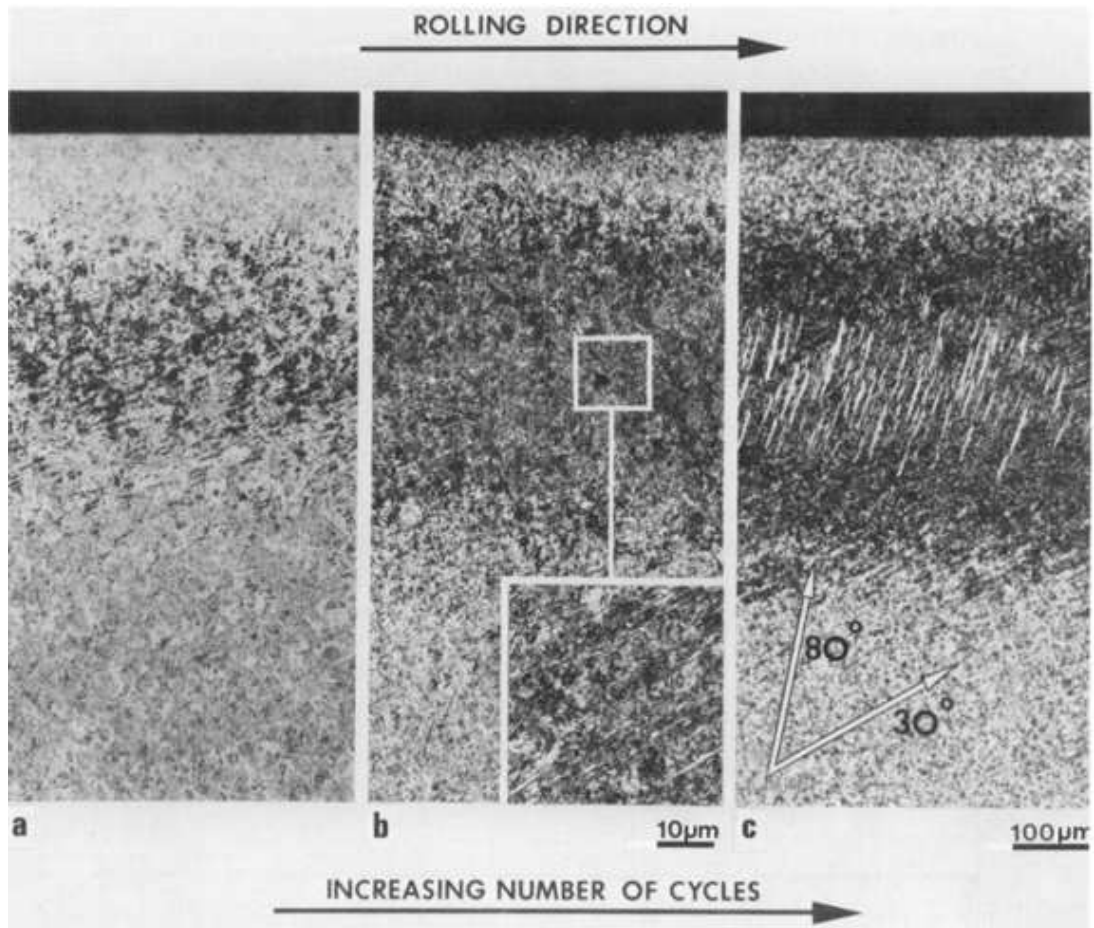


**Figure 2.** Progressive alteration of the microstructure in the subsurface region of a martensitic ball bearing as a result of rolling contact fatigue. (a) DER in early stage, (b) fully developed DER and Low Angle ( $30^\circ$ ) Bands (LABs). The insert shows a more detailed view of the DER and the LABs, (c) Late decay stage showing the DER,  $30^\circ$  and  $80^\circ$  bands. Taken from [14].

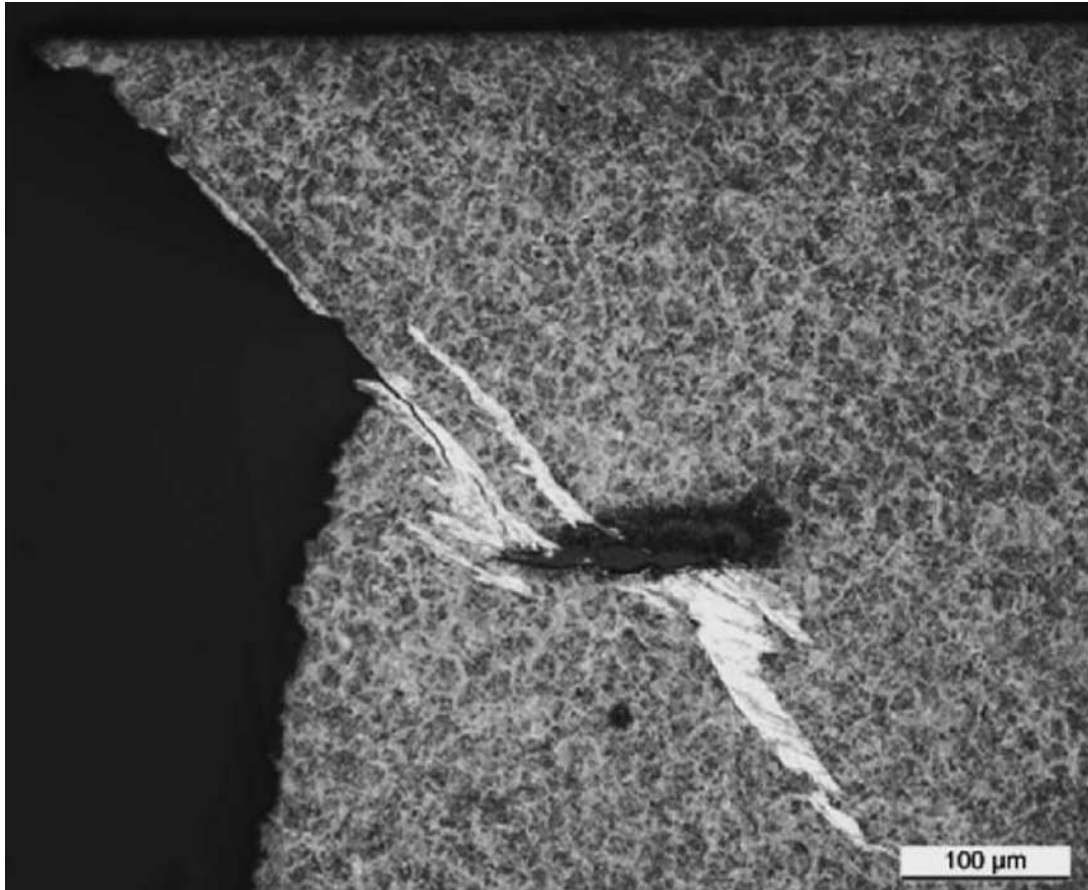


**Figure 3.** Butterfly feature with White Etching Matter (WEM) connected to a crack. Bearing steel subjected to fatigue loading. Taken from [13](#).

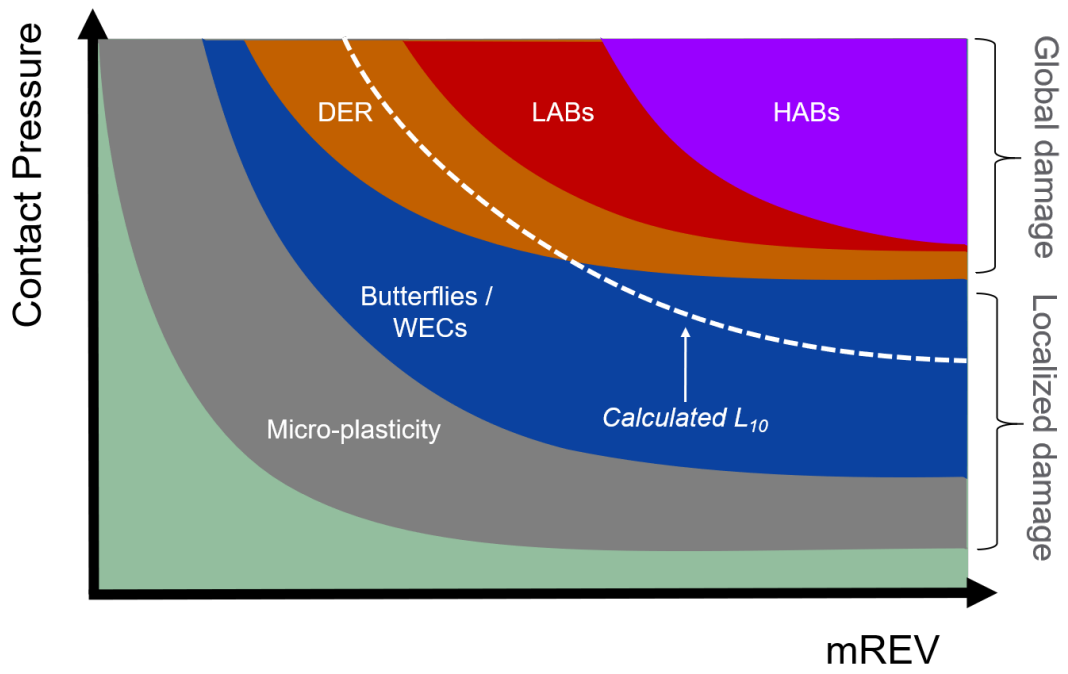


**Figure 4.** Subsurface fatigue damage map for martensitic bearings. The coloured bands indicate schematically the start of each specific mechanism. In the horizontal axis, we show the number of stress cycles in millions of revolutions (mREV).

[16].

## 2. Characterisation of the altered microstructure

Sample preparation for metallographic investigations of the “Dark Etching Regions” (DERs) produced by Rolling Contact Fatigue (RCF) is typically performed on both cross (transverse) and parallel sections. Figure 5 shows the convention for the naming of sections of the inner ring of a typical bearing.

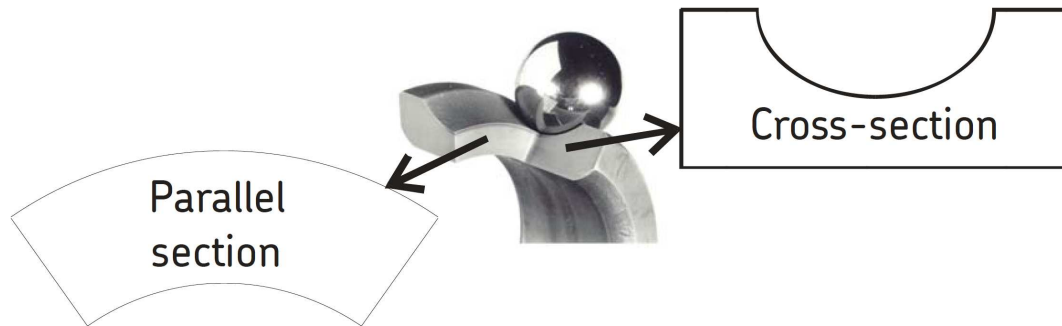


Figure 5. Directions of view on inner raceway after sectioning.

As shown schematically in Figure 6 DERs have a half-moon or sickle-like shape when the sectioning is performed on the cross-section of a bearing’s inner ring. When parallel sectioning is performed, researchers always aim to investigate the microstructure at the centre of the sickle. However, the sickle shape is not always symmetric; heavy loads can cause misalignment of the shaft held by the bearings, generating non-symmetrical loads. For instance, in the tests done on deep groove ball bearings in a traditional SKF R2 test machine set-up [17], the sickle shape turned out not to be symmetric [18]. For this reason, the observation of a representative microstructure of DERs with parallel sectioning is difficult to obtain without careful sectioning and determination of the angle of misalignment.

Typically the overall shape of the DERs, the rate of microstructure alteration, and their position with respect to the rolling raceway varies with the experimental setup. In Figure 6 we schematically show some dimensional parameters that will allow us to characterise the geometry of a typical DER in the inner ring of a bearing. We note that DERs have also been obtained in other types of contacts, such as ball-on-ball point contact [20].

## 3. Factors that affect the formation of DERs

In the absence of stress risers in the subsurface (such as impurities and inclusions) cracks tend not to form and, hence, the only fatigue damage expected on the stressed volume is the alteration of the microstructure [14,21-27]. This region that suffers progressive microstructural alterations is named after its etching characteristics relative to the original microstructure when observed on the optical microscope. It is called

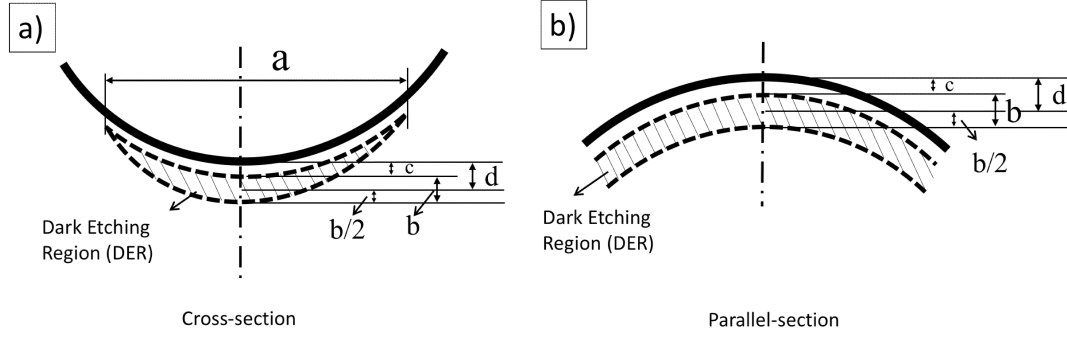


**Figure 6.** Schematic diagram of the DER of an inner ring shown along a) the cross section and b) parallel section. We introduce also the terminology of dome some common distances:  $a$ =Width of the DER,  $b$ =Thickness of the DER,  $c$ =Thickness of unaffected region just below raceway surface,  $d$ =Distance between the raceway surface and the position of maximum resolved orthogonal shear stress [19].

**Table 1.** Chemical composition of ASTM 52100 bearing steel

C	Mn	P	S	Si	Ni	Cr	Cu	Mo
0.93-1.05	0.25-0.45	0.025	0.015	0.15-0.35	0.25	1.35-1.60	0.30	0.10

the DER because it appears darker compared to the surrounding microstructure, indicating that it is more reactive to the etchant (Nital) that is typically used to reveal the microstructure of steel. It occurs beneath the raceway and over the whole circumference of the bearing ring. Apart from inner rings, DERs have also been observed in various types of specimens and components that have been subject to rolling contact fatigue [20,28,30].

We have identified in the literature four basic factors that promote the development of DERs. These are:

- (1) the susceptibility of the initial microstructure [31-33]
- (2) the magnitude of the contact pressure [19,34,35]
- (3) the number of stress cycles [18,19]
- (4) the operating temperature [29,31,35]

### 3.1. Initial microstructure

The nominal composition of ASTM 52100 bearing steel is presented in Table 1. The production of ball bearings starts with a spheroidising heat treatment to soften the steel, to render machining possible. The machined bearings are then heat treated to produce a martensitic microstructure which is subsequently tempered at low temperature. In the martensitic hardened and tempered condition (Figure 7, schematic made by the authors), bearing steel consists of at least four different phases: (1) dispersed residual cementite, (2) retained austenite, (3) a tempered martensitic matrix and (4) tempered transition carbides, such as epsilon carbide and tempered cementite, embedded in the martensitic matrix. The dispersed residual cementite is enriched with Cr and Mn. It has a chemical formula of  $M_3C$ , where M stands for metal (Fe atoms can be replaced by Mn and/or Cr atoms). In contrast, the tempered cementite is not enriched with Cr or Mn.

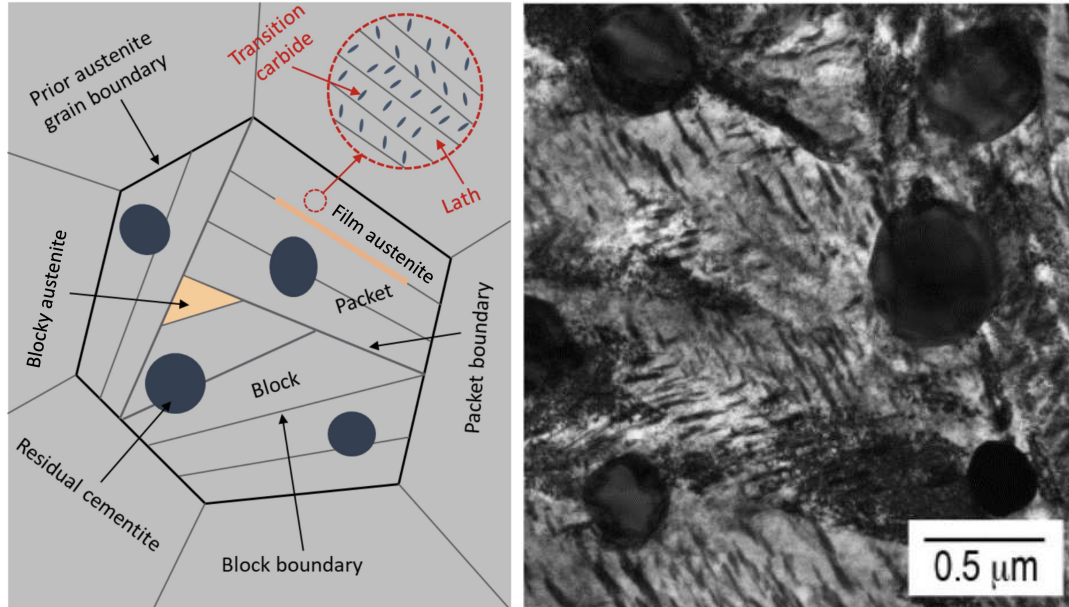


**Figure 7.** Microstructure of martensitic bearing steel: (left) schematic representation of the main features in the microstructure; (right) TEM (transmission electron microscopy) picture of AISI 52100 (100Cr6) bearing steel hardened and tempered at 160 °C for 2 hours [36].

Austenitisation is usually performed at about 840–870 °C. During this process a fraction of the spheroidised cementite dissolves and leads to carbon enrichment of austenite. There is about 0.6–0.65 wt% of carbon in the austenite at the end of the austenitisation process. Upon quenching in oil, martensite forms. After low-temperature tempering (160–270 °C), transition carbides and tempered cementite precipitate and about 5–15 vol% of austenite is retained [10][18].

### 3.1.1. Retained austenite

The transformation of austenite during rolling contact fatigue has been investigated by Voskamp [18]. Figure 8 shows the effect of contact pressure on the amount of decomposed retained austenite as a function of the number of stress cycles. Three stages were identified. The transformation of austenite detected during the shakedown stage (Stage 1) is most likely stress-assisted [18][37][39], since the rate of transformation of austenite is a linear function of the number of stress cycles. Furthermore, the length/duration of the shakedown stage is independent of the applied load. The higher the stress applied, the more substantial the amount of retained austenite transformed at this stage. The transformation of austenite is expected to alter the build-up of residual stresses in the bearing [15].

No further austenite transformation is detected during Stage 2 (steady state) of rolling contact fatigue. The duration of the Stage 2 becomes shorter with increased contact pressure. During the second stage the energy dissipated from cyclic stressing is of a too low level to cause softening of the tempered martensitic microstructure [18].

The instability state (Stage 3) is characterised by a drastic decrease of the content of retained austenite with increasing number of stress cycles. In Figures 9a and b, it is indicated that the decomposition of austenite can happen simultaneously to the formation of DER. We also show in Figure 9b that, with a contact pressure of 3.7 GPa

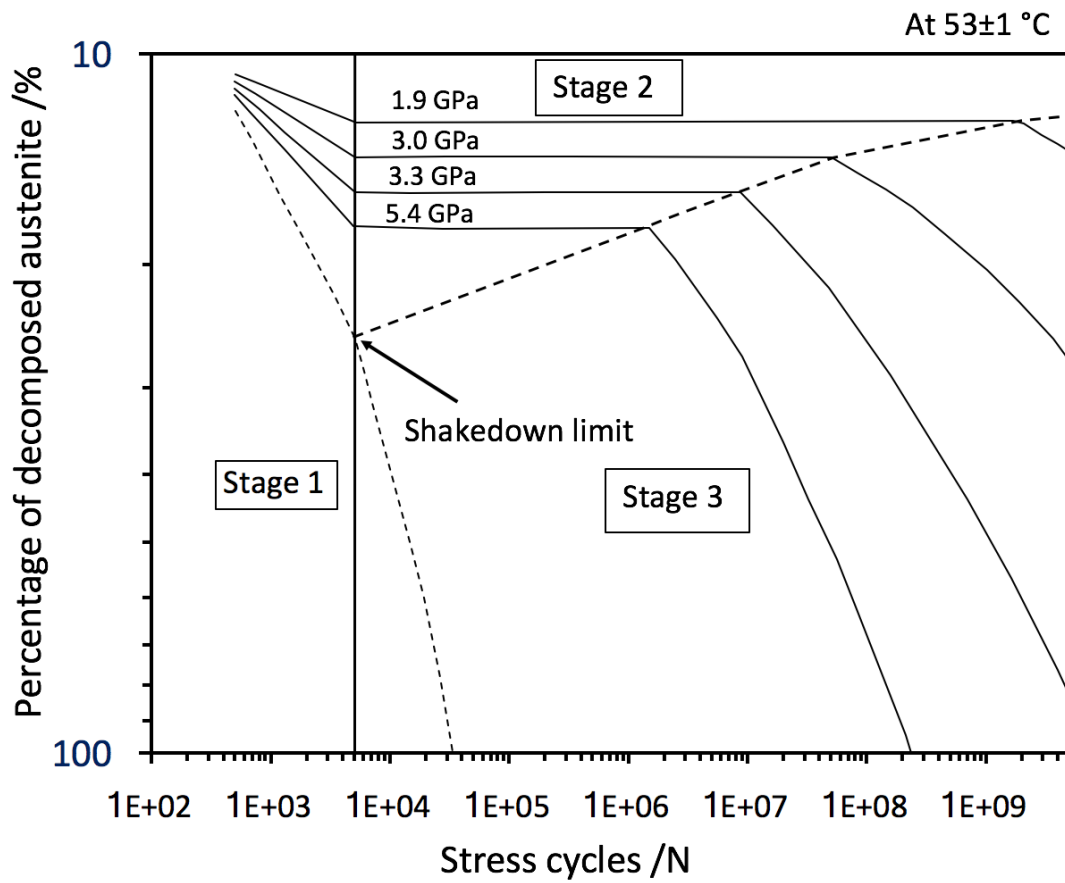


**Figure 8.** Effect of contact pressure on the amount of retained austenite decomposition as a function of stress cycle. Retained austenite is measured at 0.2 mm below the raceway. [18]

after a sufficiently large number of stress cycles, a total decomposition of retained austenite can occur in the subsurface region subjected to the higher stresses.

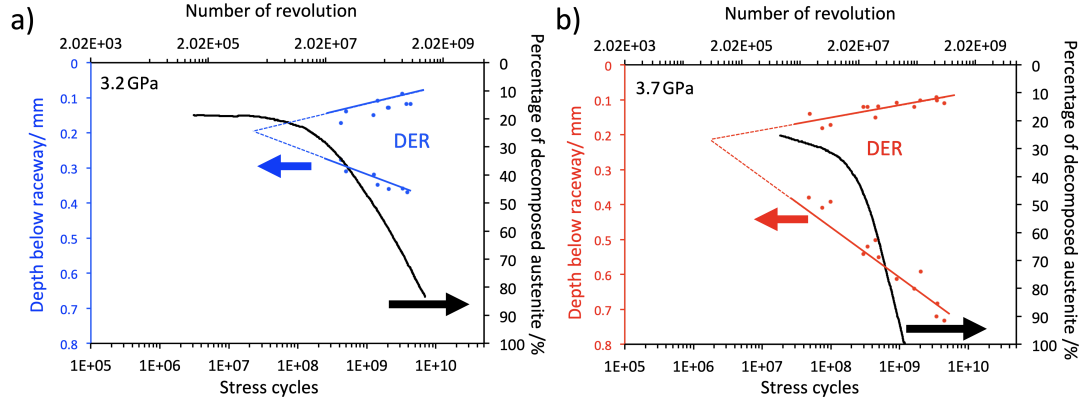


**Figure 9.** Effect of the number of stress cycles on the decomposed retained austenite and DER formation. Retained austenite is measured at the depth of 0.2 mm for both a) 3.2 GPa and b) 3.7 GPa [18].

### 3.1.2. Effect of silicon on the formation of DERs

The addition of silicon to bearing steels has been reported to prevent the formation of DERs by various studies [33,38,40,41]. However, the nature of the preventive mechanism of DER formation by silicon has never been discussed. Silicon is known to prevent austenite decomposition during bainite transformation as it hinders cementite formation [42]. Furthermore, silicon addition is also known to inhibit the growth of  $\epsilon$ -carbides [43]. The presence of fine  $\epsilon$ -carbides in silicon-added tempered martensitic matrix could prevent the rearrangement of dislocations and, hence, delay the DER formation.

By measuring the depth of the groove formed on the raceway, Andersson et al. [44] have shown that the addition of both Si and Mn, and the reduction of Cr in bearing steels are beneficial for the improvement of the microstructural stability during rolling contact fatigue, and, hence, the prevention of DER formation. This is an indirect method of detecting the formation of DERs.

It has also been reported that Si tends to partition to the matrix, and not to the carbides [45]. When Si is present in the matrix, C interacts with it and the diffusivity of C is reduced [46]. The two main reasons are (1) the strong repulsion between C and Si atoms in the first and second neighbor shells of Si, which diminishes the number of diffusion paths for C, as C is blocked from accessing sites close to Si; and (2) a weak attraction from the third to the sixth shell of Si that tends to trap C and impede its free motion. Since C diffusion is one of the main drivers for the formation of DERs, it is expected that the reduction of the diffusivity of C caused by the presence of Si, will delay the formation of DERs.

### 3.1.3. Crystal orientation

The initial formation of DERs is probably affected by the local crystal orientation, since it is observed that the initial appearance of the DERs is not uniform throughout the

stressed volume but appears in patches. The variable orientation of the crystals plays a role in the so called “intrusion/extrusion” mechanism for the formation of DERs proposed by Bush et al. [31]. They suggest that the whole process of microstructural alterations begins when a few martensite crystallites in the vicinity of a carbide yield, generating pile-ups of dislocations at the carbide/matrix interfaces (See Section 5.2).

### 3.2. Operating conditions

Operating conditions also have an influence on the formation of DERs. High contact pressures promote early formation of DERs, as shown in Figure 10. When the contact pressure is higher, the formation of the DERs starts after a lower number of stress cycles and the size of the DERs (in depth) increases with the contact pressure and the number of stress cycles. Similarly, there is evidence showing that higher operating temperatures accelerate the formation of DERs.

#### 3.2.1. Contact pressure and number of stress cycles

The microstructural alterations that lead to the formation of DERs are initiated within the subsurface volume subject to rolling contact stress, see Figure 1. They start at the region where the maximum resolved shear stress is experienced [18] and spreads to the rest of the stressed volume as the number of stress cycles increases [18,19,27,31]. In recent articles, it is argued that the DERs do not form within the maximum shear stress region [11], but that they are closely related to the von Mises stresses [20]. Figure 10 shows the size of the DER as a function of the number of stress cycles at two different contact pressures, indicating that its formation depends both on the stress and the number of stress cycles [18,19]. Higher contact pressures promote early DER formation [18]. Figure 10 also shows the effect of contact pressure on the size of the DER as a function of the number of stress cycles. The thickness of the DER increases asymmetrically towards greater depths with increasing number of stress cycles.

The formation of DERs is manifested by changes in hardness. The effects of the contact pressure and number of stress cycles on the change of hardness of DERs compared to the parent material are not conclusive when looking at the results reported in the literature, and it is even more mystifying when different operating temperatures are used.

Microhardness measurements on the DERs performed by Swahn et al. [14] and Kuroda [28] were compiled by the authors and are presented in Figure 11a and 11b, respectively. Interestingly, we see that Swahn et al. report softening of the microstructure, while Kuroda reports hardening. We note that the sectioning of the bearing for the hardness measurements was done differently in both articles.

Limited evidence has shown that high contact pressure, above 5 GPa, leads to the increase of hardness, see Figure 11 and Figure 12. At lower contact pressures, hardness in DERs has been reported to increase, decrease and to remain unchanged compared to the parent material, see Figure 11, Figure 12 and Figure 13. Figure 11 also shows that it has been reported that with increasing number of stress cycles, the hardness of the DER (a) decreases [25] or (b) increases [28].

It is still not clear why sometimes hardening or softening is measured in the DER. We can only speculate that due to the anisotropic nature of the DERs, there is an influence of the section where the hardness measurements are performed. El Laithy et al. hypothesised that there is a competition between softening due to the decay of martensite, and hardening due to the decay of austenite [11].

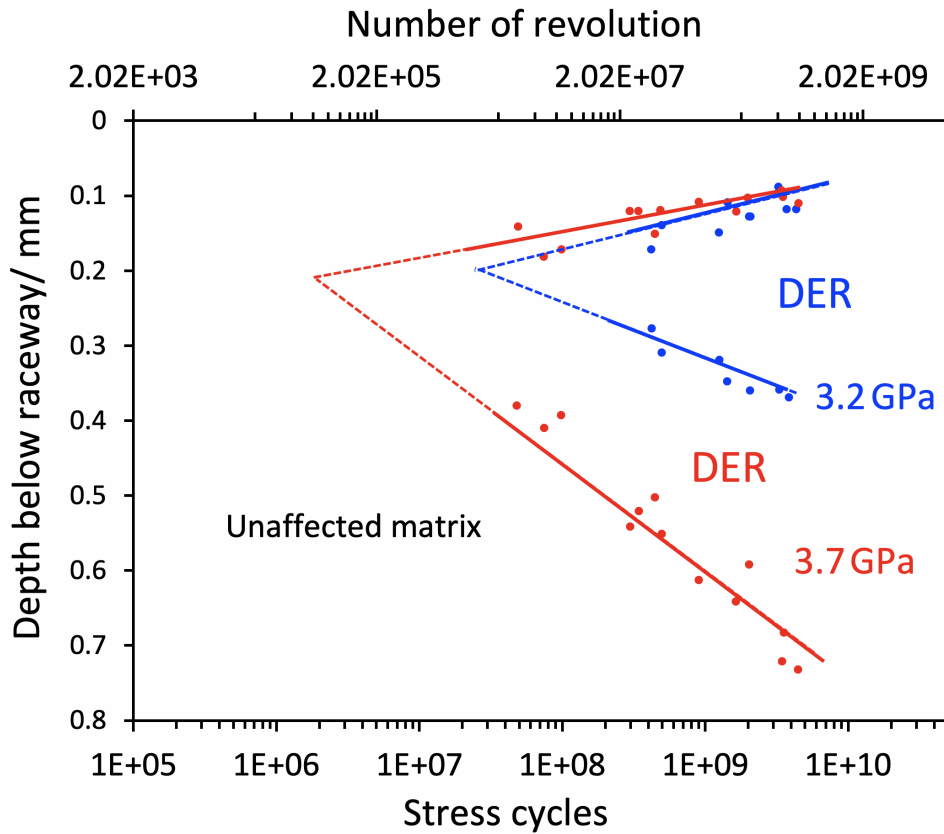


**Figure 10.** Depth distribution of DERs at two different pressures 3.2 GPa and 3.7 GPa. The boundaries between the DER and the matrix were measured from optical micrographs. Note that the DER does not extend to the surface [18].

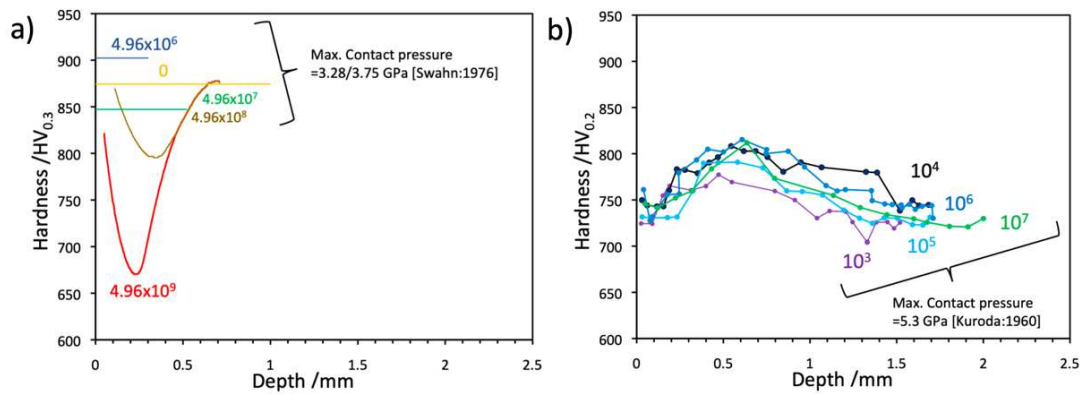


**Figure 11.** Microhardness as a function of depth under the raceway in inner rings before testing and after specified number of stress cycles,  $N$ . The data plotted are from two different works a) Swahn [25] and b) Kuroda [28] using two different contact pressures. The material used for both experiments are of the same grade but the bearing setup was different.

In Figure 12 we present the effect of the contact pressure, the initial hardness, and the number of cycles on the hardness of the affected region as a function of the depth. The figure is adapted from the work of [29]. Although it was noted that high contact pressures increase the hardness of the material, the effect of low contact pressures remains unclear.

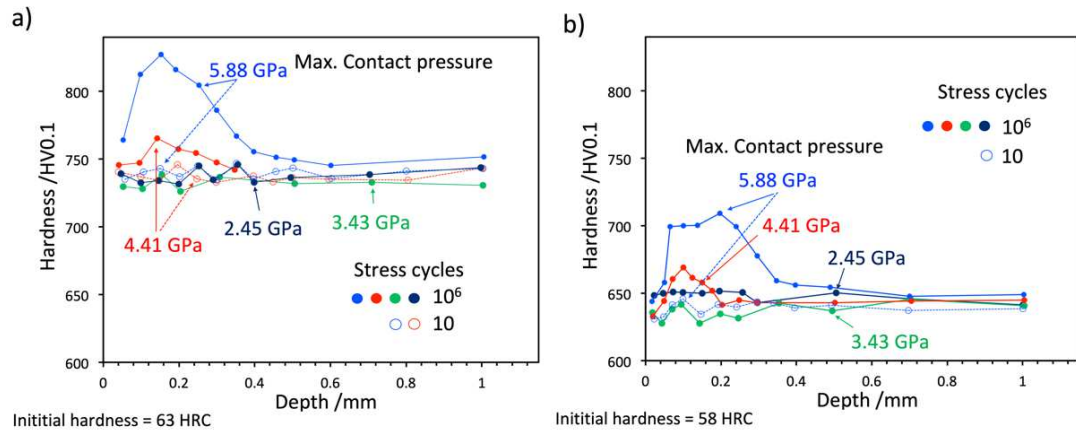


**Figure 12.** Change in hardness with depth due to different initial hardness, contact pressure and number of stress cycles. Hardness measured from the cross section of the rod. Experiment on ball on rod with 38 mm diameter, no operating temperature is reported. From [29].

Figure 13 shows the change in DER hardness after rolling contact at pressures of 2.8, 3.3 and 3.8 GPa. It is shown that while the hardness of the DER increases, the width of the Full Width Half Maximum (FWHM) of the (211) ferrite peak decreases, indicating a reduction of the dislocation density and tetragonality in the DER [47].

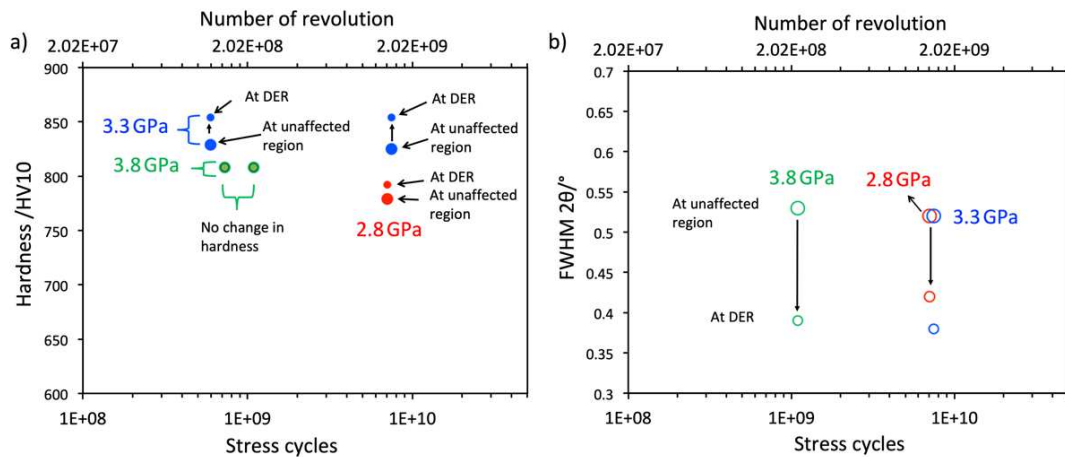
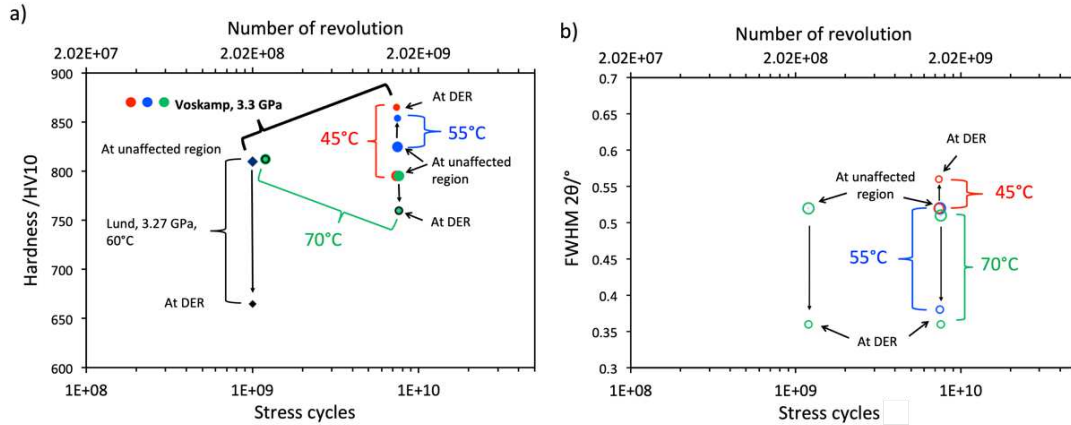


**Figure 13.** Effect rolling contact pressure on the microhardness change and X-ray peak broadening as a function of the number of stress cycles at constant temperature of 55 °C. The small symbol indicates the hardness measured at DER, while the large symbol indicates the hardness measured at the unaffected region. No hardness change is observed on the DER when the contact stress is 3.8 GPa [18].

### 3.2.2. Temperature

It has been reported in the literature that high operating temperatures accelerate the formation of DERs [23][29][48]. Depending on the bearing design, the amplitude of the contact pressure and the running speed, the heat generated by friction might not be dissipated instantaneously; this additional thermal energy increases the bearing operating temperature. Additionally, if there is an external heat source, a higher operating bearing temperature can be expected.

The effect of temperature on the change of hardness of the DER is mystifying. As shown in Figure 14 with a very similar contact pressure, Lund [49] reported a significant decrease in hardness when the operating temperature is 60 °C. At a similar contact pressure and stress cycles, but at a higher operating temperature of 70 °C, Voskamp [18] reported no change in hardness in the DER. Voskamp [18] also showed that at a contact pressure of 3.3 GPa, after  $7.48 \times 10^9$  stress cycles and at an operating temperature of 70 °C, the hardness of the DER decreased; conversely, he showed that at operating temperatures of 45 °C and 55 °C there is an increase in hardness.



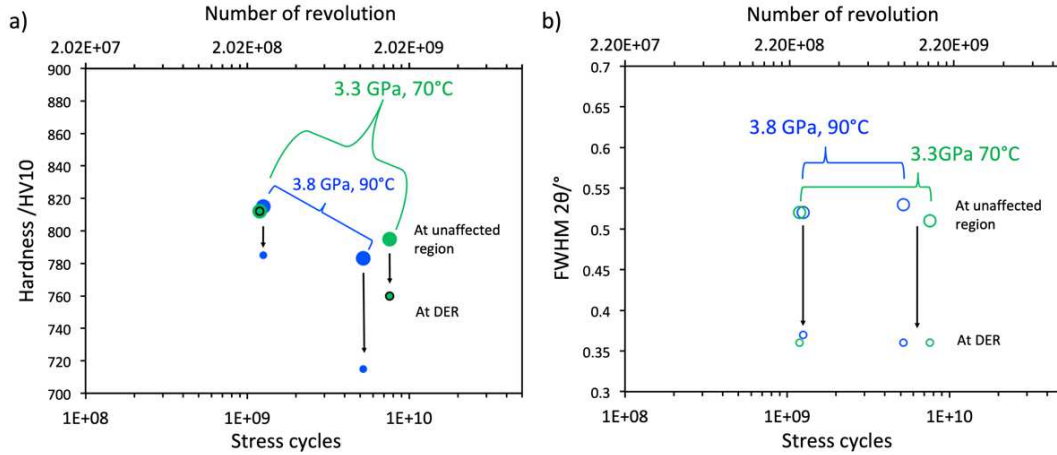
**Figure 14.** Effect of bearing operating temperature on the microhardness change and X-ray peak broadening as a function of stress cycle at contact pressure of about 3.3 GPa [18]. The small symbol indicates the hardness measured at DER, while the large symbol indicates the hardness measured at the unaffected region. No hardness change is observed on the DER at stress cycle of  $1.2 \times 10^9$  at 70°C. At 70°C, the small green circle with black line is used to indicate the hardness at the DER.

Figure 15a shows that the hardness of the DER is unchanged when testing is performed at 3.3 GPa and 70 °C during  $1.2 \times 10^9$  stress cycles. However, at a higher contact pressure of 3.8 GPa and higher temperature of 90 °C, the hardness of the DER decreases.

## 4. Microstructural behaviour and phenomena

### 4.1. Microstructure of the DERs

This review is further complicated by the different terms used by investigators throughout the time to describe the same microstructure. The origin of dark etching regions is essentially due to the formation of ferrite microbands and elongated ferrite grains. The terms “ferrite microband” and “elongated ferrite” are thought to be the most ac-



**Figure 15.** Effect of contact pressure and bearing operating temperature on the microhardness change and X-ray peak broadening as a function of stress cycles at contact pressure of about 3.3 GPa and 3.8 GPa at 90 °C and at 70 °C [18]. Hardness and FWHM values measured at the unaffected region are indicated with large circles, while hardness and FWHM values measured at the DER are marked with small circles. The small green circles are with the black line to indicate that there is no change when the contact stress is at 3.3 GPa operating at 70° at  $1.2 \times 10^9$  stress cycles. The green and blue circles show the different contact pressures and operating temperatures.

curate representations of the structure observed via optical and electron microscope. The formation of ferrite microbands and elongated ferrite is related to the dislocation rearrangement under cyclic applied stress. Ferrite microbands bear a superficial resemblance to the persistent slip bands (PSB) observed in single crystal cyclic fatigue tests [50].

The movement and rearrangement of dislocations during the formation of ferrite microbands and elongated ferrite dissolve residual cementite [18] (see Figures 28 and 30). Nevertheless, it is still argued in the literature what happens to the temper carbides; do they coarsen? or do they dissolve?. It has been suggested in the work of Fu et al. [51] that the presence of the transition carbides surrounded by the DER is the evidence of carbon migration from parent (tempered) martensite towards the pre-existing tempered carbides.

#### 4.1.1. Ferrite microbands and nanocrystalline ferrite

The formation of DERs is location dependent. Their initial formation is affected by the crystal orientation of the martensite packet and their further growth is related to the Hertzian stress distribution within the stressed volume. Due to their complexity, the microstructural observation of DERs needs a combination of different and complementary microscopy techniques for detailed characterisation.

Observations under the Light Optical Microscope (LOM) are used in virtually every investigation of DERs. In fact, DERs are named after their etching characteristics: DERs are more reactive to the etchant and appear darker relative to the unaffected surrounding microstructure of tempered martensite and residual cementite (retained austenite and tempered carbides are not observable by optical microscopy). However, due to the low resolution of optical microscopy, the microscope cannot reveal any significant details other than the position and shape of the DERs. Light optical mi-

crosscopy is generally used to measure the size of the DERs with respect to contact pressure and number of stress cycles (Figure 10).

The emergence of DERs as observed in a light microscope is due to the differences in elevation and roughness caused by the preferential etching. A region would appear dark when there is more scattering of the light, i.e. less light is reflected into the objective lens of the light microscope. Typically, this region is rougher than the region that appears lighter. The reason this region is rougher is due to the presence of smaller grain sizes or multiple phases or more interfaces.

To fully characterise the microstructural alterations in DERs, Scanning Electron Microscope (SEM) in combination with Focused Ion Beam (FIB) (which allows the production of position specific TEM lamella) has been used [52,53]. Such an advance in the characterisation equipment has only been available in recent years and should be utilised to improve the understanding of the structure of DERs.

The development of the DERs starts with the formation of ferrite microbands. The terms used in the literature to describe the ferrite microbands [54] include ferrite [14], slip motions [15], troostite/mechanical troostite [23,24,55,56], tempered martensite [31,55,57], upper bainite/ microslip/ deformation bands [31], dark needles [29], needle like structure [28], acicular structures [58] and elongated cells [35]. The term “martensite decay” is commonly used when the actual product of microstructure alteration is unclear. The use of many terms to describe one single microstructure indicates the lack of understanding of the topic and show that this has been the subject of much speculation [31].

The ferrite microbands extend across martensite plate boundaries [54]. The microbands run in the same direction, that is, they are parallel to the surface when viewed on a transverse cut (parallel section) [54]. The macroscopic lining up is due to the applied stress. According to reference [54] the presence of this alignment of the microbands confirms that their formation is caused by the applied strain during RCF and is not due to local heating effects from the release of strain energy.

Detection of DERs show patches [26,54] of densely spaced microbands within an unaltered matrix. When looking at the cross section of a rolling bearing (Figure 16), the microbands seem to be aligned parallel to the raceway on both sides of the symmetry plane. At the middle section of the raceway, the DER microbands do not possess any unique orientation and multivariant microbands are observed [15,51]. Fu et al. [51] prepared TEM lamella in the DER from the parallel section and found multivariant ferrite microbands.

In the later stage of the formation of DERs, regions of homogeneous nanocrystalline ferritic structure can be observed [32]. Other terms used for the homogeneous nanocrystalline ferritic structure include: polycrystal cell [35], cell ferrite [26], cell-like structure [32], heavily deformed ferrite [59] and globular ferrite [60]. At an appropriate magnification, electron diffraction patterns obtained from this area produce a ring structure that indicates the presence of multiple grains with random crystal orientations. There is abundant evidence [18,25,27,32,48,60,61] indicating that the 30° WEBs and the 80° WEBs are essentially comprised of nanocrystalline ferrite.

The earliest evidence of dislocation cell formation in fatigue-damaged microstructures was provided by Osterlund [26] using Transmission Electron Microscopy (TEM). Figure 17 shows TEM images of the microstructure of dark and white etching areas resulting from a high contact pressure (5.5 GPa) bearing test. The dark etching region shown in this case is textured and the grain size is relatively large compared to the nano-poly-crystalline ferrite present in the white etching regions. Similar to the White Etching Matter (WEM) investigated by Kang et al. [62], the residual cementite is not

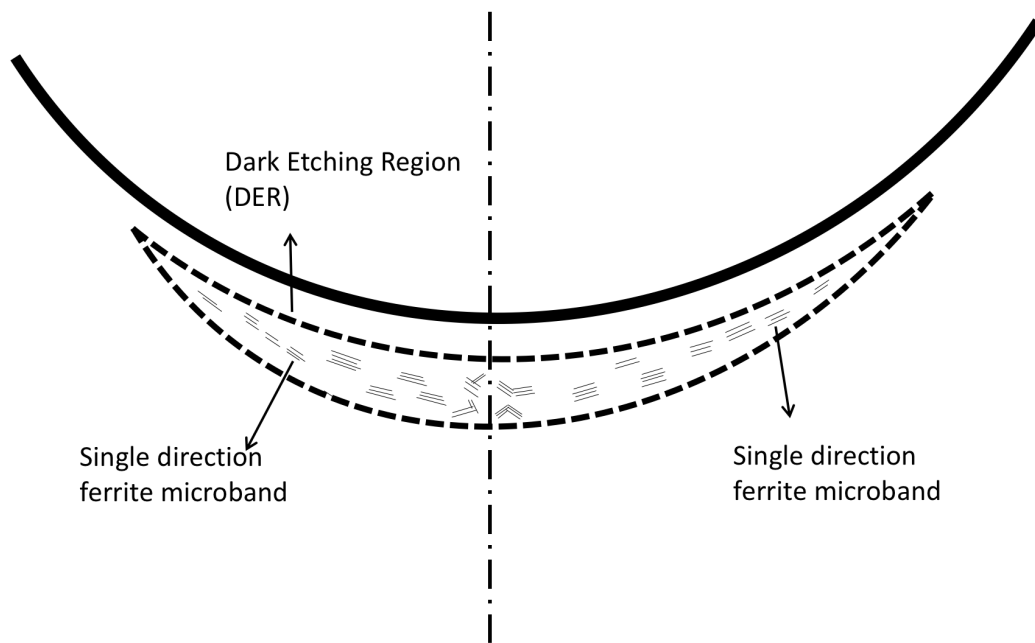


**Figure 16.** The effect of position relative to the centre of the sickle on the directionality (single variant or multivariant) of the microbands. At the centre, there are multiple variants and do not possess any unique directionality. At both sides of the symmetry plane, single variant microbands that are parallel to the rolling surface are observed. Drawing based on the description by King [54](#) and Fu [51](#).

fully dissolved within the 80° bands [18] (See Figure 18b). Notice that not all the nano-poly-crystalline ferrite has the same contrast, indicating that there are misorientations across cell walls (See Figure 17c and Figure 18a). The change of the diffraction pattern spots from arc to ring in figure 17a and c further indicate the increase misorientations of the tempered martensite/ferrite grain within the dark etching and the white etching region. Figure 17b and d show the change of the tempered martensite/ferrite morphology in the dark etching region to equiaxed nano-ferrite.

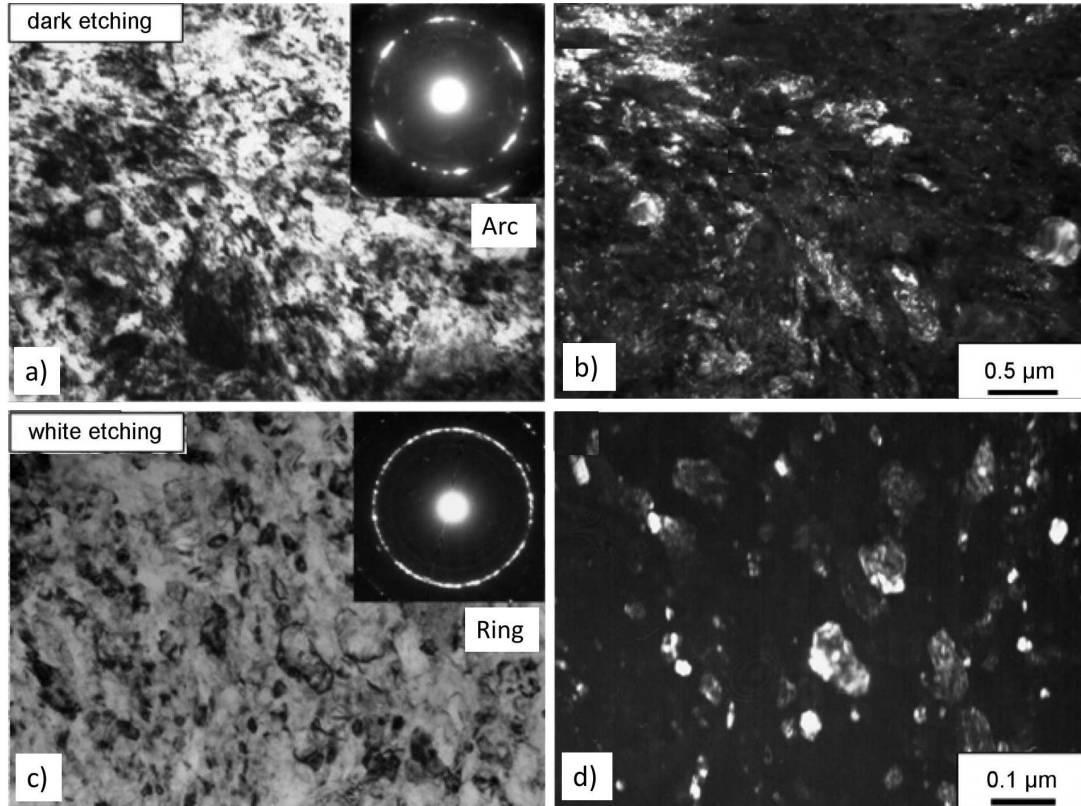


**Figure 17.** a) and b) Bright field and dark field transmission electron microscope image of dark etching region located 0.25 mm below the raceway. c) and d) Bright field and dark field transmission electron microscope image of the white-etching band. After rolling contact fatigue testing at the contact pressure of 5.5 GPa for 4.3 million cycles at 130 °C. The 52100 steel was austenitised at 840 °C for 40 min and tempered at 170 °C for 2 h before the bearing test [48].

Ferrite microbands in DERs transform into nanocrystalline ferrite as the number of rolling cycles increases. Table 2 shows the effect of contact pressure, number of stress cycles, and operating temperature on the measured nanocrystalline ferrite grain size within the 80° WEBs. It is shown that the increase in the contact pressure and the operating temperature with prolonged stress cycling, decreases the nanocrystalline ferrite grain size. At a low contact pressure of 3.72 GPa and after  $2.48 \times 10^9$  stress cycles the measured grain size of the nanocrystalline ferrite is about  $188 \pm 16$  nm; the grain size is reduced to  $127 \pm 16$  nm after  $3.27 \times 10^9$  stress cycles at the same contact pressure. This significant grain refinement is observed at the high contact pressure of 5.5 GPa and high temperature of 130 °C; the grain size is reduced to about  $35 \pm 6$  nm after merely  $2.3 \times 10^7$  stress cycles.

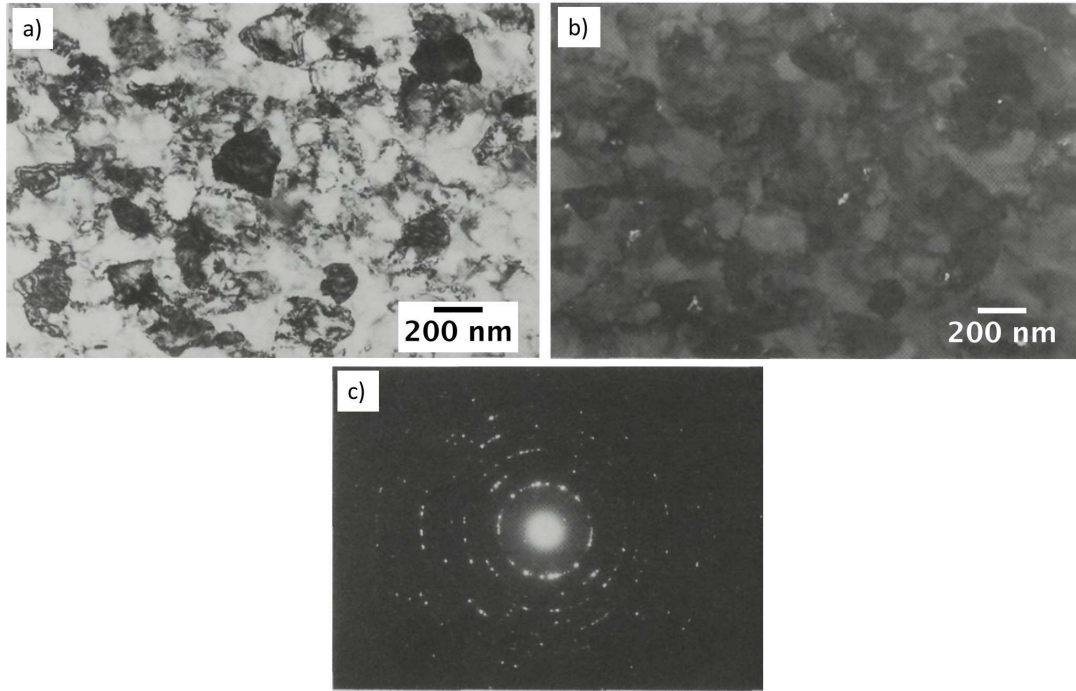


**Figure 18.** Transmission electron micrograph of the ferrite cell and cementite in 80° bands. After rolling contact fatigue testing at contact pressure of 3.72 GPa for  $3.27 \times 10^9$  stress cycles at 53 °C [18]. a) Bright field TEM image shows overall fine equiaxed ferrite grain size within the bands. b) Dark field TEM image taken using a cementite diffraction spot in c). The undissolved cementite is in white while the equiaxed ferrite is in dark.

**Table 2.** Effect of contact pressure, number of stress cycle, operating temperature on ferrite cell size at 80° white etching bands (WEBs). The measurement of the cell size is done using the linear intercept method.

Contact pressure [GPa]	Stress cycles	Operating temperature °C	Cell size [nm]	Reference
3.72	$2.48 \times 10^9$	50–55	$188 \pm 16$	[27]
3.72	$3.27 \times 10^9$	53	$127 \pm 16$	[18]
5.5	$2.30 \times 10^7$	130	$35 \pm 16$	[48]

The sizes of the 30° and 80° WEBs (especially the length) are significantly larger than those of typical prior austenite grains with no observable deviation. This indicates that the growth of 30° and 80° WEBs is not affected by the crystal orientation of the prior austenite grains.

#### 4.1.2. Elongated Ferrite

Another prominent feature visible in the DERs is the elongated ferrite. Elongated ferrite is also formed within the martensitic matrix structure during rolling contact fatigue but appears as individual features and not grouped like the ferrite microbands (see Figure 19). The elongated ferrite appears as a dark line (essentially parallel to the raceway) when observed in cross-section view in the SEM. Elongated ferrite has been described as elongated thin “stringers” [31]. Other terms have been used for this feature including elongated cell [35] and elongated thin “stringers” [31]. It is not clear if the formation mechanisms of both ferrite microbands and elongated ferrite are related. It may be that the ferrite microbands start as elongated ferrite but become ferrite microbands when multiple elongated ferrite features form close to each other, while isolated elongated ferrite would survive and grow into large elongated ferrite grains.

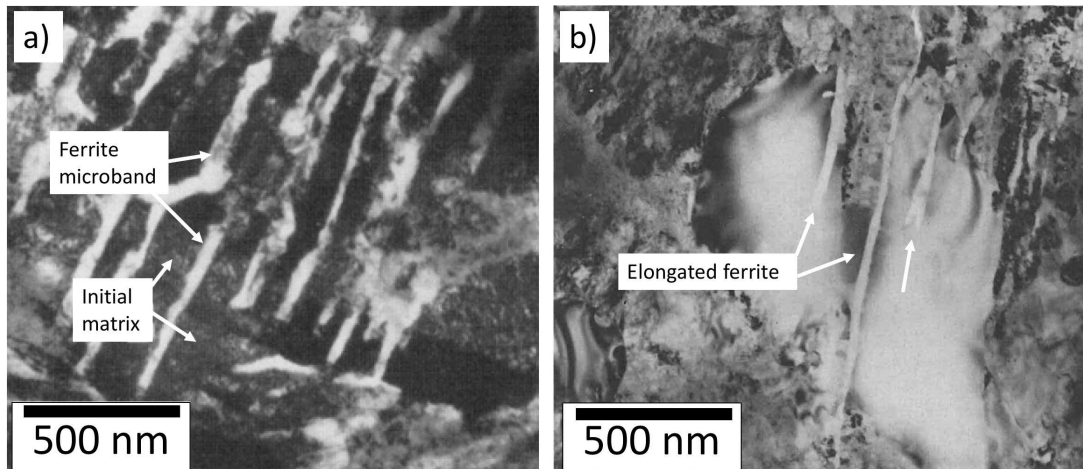


**Figure 19.** Transmission electron micrograph of a) ferrite microbands [25] and b) elongated ferrite [14].

There is an indication that elongated ferrite grows to form a large ferrite grains at the 30° and 80° WEBs [60]. The elongated ferrite is composed of thin ferrite plates and lies at about 30° or 80° to the raceway surface when observed in the parallel section. When viewed at the cross-section, the bands are parallel to the raceway surface. With increasing number of cycles, they can grow to a certain size. The elongated ferrite is not polycrystalline and is the result of texture formation as detected by Voskamp [18].

30° and 80° WEBs appear white when observed in the optical microscope. Their internal structure can be very heterogeneous across the thickness. Both 30° and 80° WEBs can be made up of polycrystalline nano size ferrite and elongated ferrite [60]. Figure 20 presents an EBSD image obtained from 30° and 80° WEBs [60] showing the distribution of elongated ferrite and nano-poly-crystalline ferrite.

Figure 21 shows a TEM image obtained from 30° WEBs [60]. While Šmeļova et

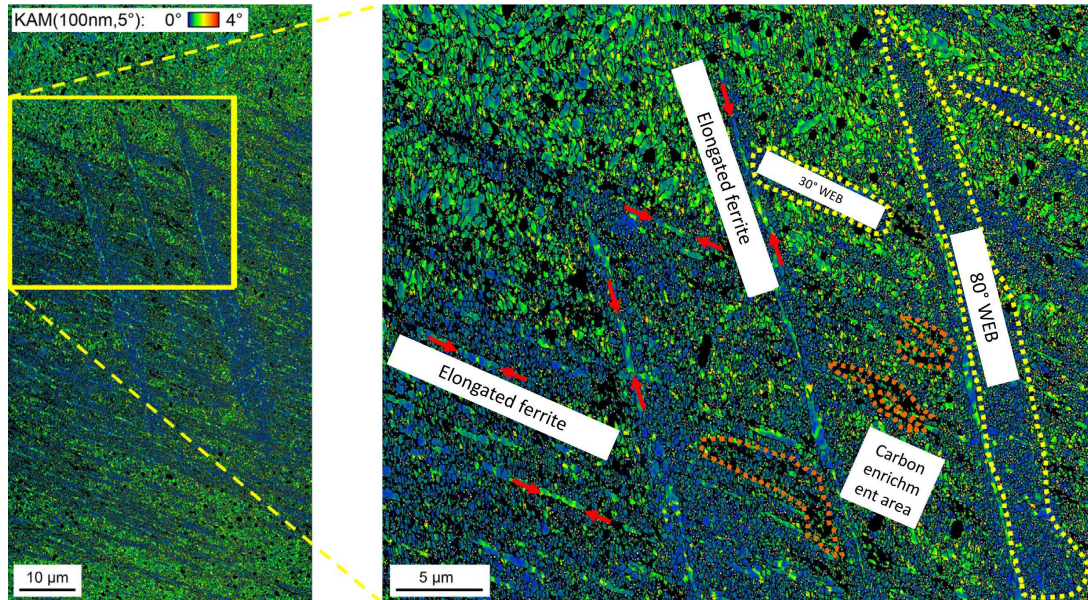


**Figure 20.** EBSD image on the distribution of elongated ferrite, nano-poly-crystalline ferrite and both 30° and 80° WEBS in a fully developed DER [60].

al. [60] claimed that the obtained diffraction pattern could not be indexed, the diffraction pattern on the 30° WEBS shown in the figure was indexed by the authors as a large ferrite crystal with lenticular cementite, surrounded by fine ferrite grains.

#### 4.1.3. Decomposition of retained austenite

The response of the as-heat-treated bearing steel to fatigue loading is not the same as that of other engineering materials. One of the factors that contribute to the fatigue behaviour is the presence of retained austenite, which is usually (but not necessarily) found in bearing steels [63]. Rolling contact fatigue is accompanied by the decomposition of retained austenite [18][37][39][59][64][65]. At low (< 15 vol%) austenite content, there is no observable change in the etching characteristics [18] even though a decrease of retained austenite is detected at the beginning (Stress cycles < 5000) of the bearing test.

The presence of retained austenite alters the response of the material right from the first stress cycles: it transforms into martensite causing an increase of the yield stress. The rapid hardening at the shakedown stage (see Stage 1, Figure 8) during rolling contact is accompanied by the transformation of retained austenite into martensite; such transformation induces an increase of the dislocation density within the freshly formed martensite [42][66].

#### 4.1.4. Dissolution or growth of residual carbides

The residual cementite is much harder than the tempered martensitic matrix in 52100 bearing steel, so it is expected to resist plastic deformation [43][67]. However, both elongated ferrite and ferrite microbands are observed to grow into the residual cementite causing it to progressively dissolve [14][31]. Furthermore, many cementite particles

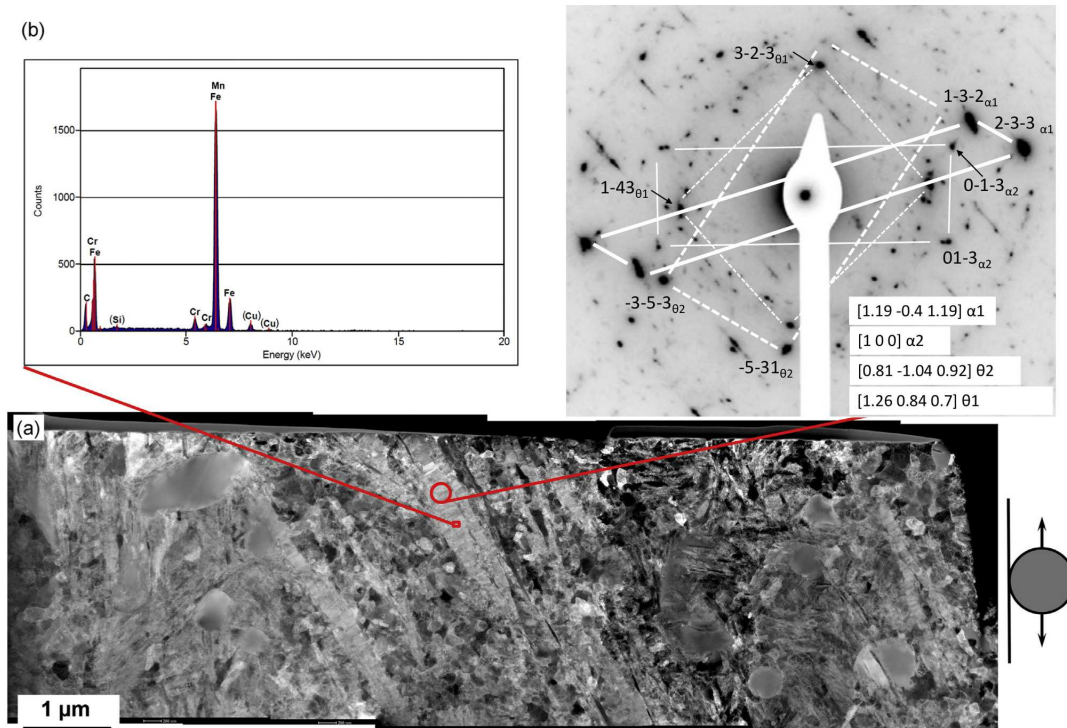


**Figure 21.** TEM analysis of 30° bands: (a) Bright field images (b) EDX spectrum on elongated ferrite; and (c) The indexed selected area diffraction pattern shows that the 30° bands/ elongated ferrite is comprised of single crystal ferrite ( $\alpha_1$ ). The second ferrite ( $\alpha_2$ ) spots are small and are not from the elongated ferrite ( $\alpha_1$ ). This is because the 'selected' area of diffraction (SAD) would include the surrounding region of elongated ferrite. Two cementite crystals were indexed most likely to be from lenticular cementite [60]. The rolling direction is in the vertical direction, as indicated by the label. The diffraction patterns were indexed by the author.

have been shown to have indistinct edges with the matrix [14,26,31,32,51], rather than a sharp and smooth interface, as observed in the quenched and tempered condition. All these observations suggest that the cementite is partially dissolved during rolling contact fatigue. The pileups of dislocations created by rolling contact fatigue are expected to be formed mainly at the martensitic matrix and at the interfaces with residual cementite. The dislocation pileups would then draw out and trap a significant amount of carbon atoms away from the cementite. The diffusion of carbon from the cementite towards the dislocations near the cementite/matrix interface is a possible mechanism for the dissolution of the cementite [68].

Partial dissolution of residual cementite during rolling contact fatigue is not caused by the breaking up or fragmentation of cementite particles [69,70], as observed during wire drawing of pearlitic steel, but by progressive dissolution by dislocation pileups and the formation of ferrite microbands and elongated ferrite. The dissolution of residual cementite does not require the diffusion of iron; only long-range carbon diffusion is required. Cementite dissolution in steel during fatigue has been reported by McGrath [71].

The partial dissolution of residual cementite allows high concentrations of carbon to migrate into dislocations and boundaries. While it has been shown that both structures can accommodate a large amount of carbon [71,72], a detailed investigation of carbon distribution inside ferrite microbands and around elongated ferrite within the DERs is yet to be performed.

#### 4.1.5. Lenticular carbides

Lenticular carbides are typically formed on the side and parallel to large WEBS [14,26,32,73]. A fully developed WEB can be 50–60  $\mu\text{m}$  in length and 10  $\mu\text{m}$  in width, while the thickness of a lenticular carbide can reach 1  $\mu\text{m}$  [74]. The emergence of WEBS after about  $10 \times 10^9$  stress cycles is typically observed in conjunction with the formation of lenticular carbides [26]. Lenticular carbides have been identified as cementite but without partition of Cr and Mn [55]. It can be hypothesised that the formation and growth of lenticular carbides adjacent to white etching bands (WEBS) is related to the dissolution of tempered carbides and residual cementite and the subsequent reprecipitation of cementite. This could be caused by the reduction of the solubility of carbon within the WEBS or when the maximum solubility of carbon in the WEBS is reached, due to the continuous dissolution of cementite within the WEBS. It has been shown that the formation of lenticular carbides is related to the partial dissolution of residual cementite and does not require the full dissolution of residual cementite within the WEB [26,32,60].

#### 4.1.6. Carbon redistribution

The redistribution of carbon within DERs has been studied using Atom Probe Tomography (APT) by Fu et al. [52]. Such an experiment was performed on an APT tip of about 50 nm in diameter and 200 nm long. The redistribution of carbon atoms is shown on reconstructed 3D atomic maps (Figure 22) where Fu et al. claimed that the carbon rich regions correspond to cementite and other transition carbides.

The shape of the precipitates in such a small size (if formed from saturated ferrite/martensite) is typically spherical or cylindrical. It is also debatable to define such fine, carbon-rich, features as carbides without any further supporting evidence like electron diffraction patterns, carbide orientation relationship with the matrix, or the

analysis of the precipitate shape and size. Further research is needed to clarify this topic.

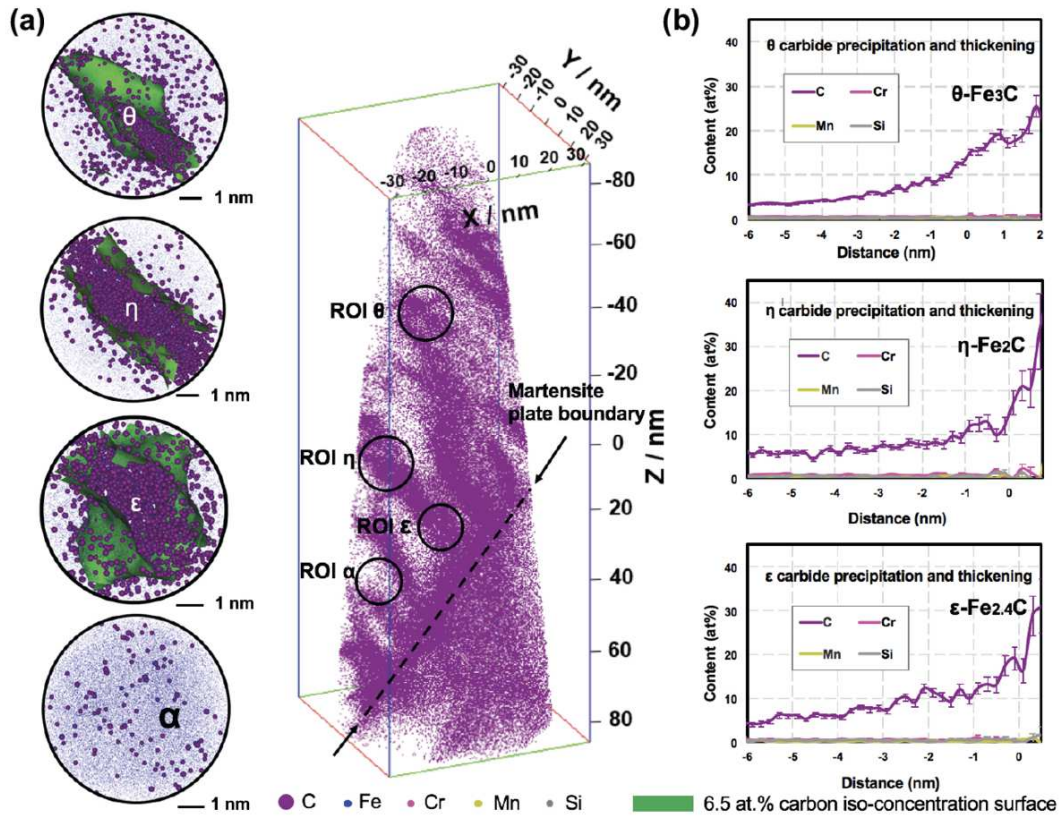


**Figure 22.** a) 3D atomic map obtained by Fu et al. [52] from DERs and the carbon distribution at selected region of interests (ROIs). (b) Proxigrams for different ROIs selected in (a).

#### 4.1.7. Dislocation density

The dislocation density can be determined by the analysis of the line broadening (FWHM) of the ferrite 211 peak, but this type of investigation is not available for bearing steels in the literature. What is currently available is a qualitative comparison (made by Voskamp [18]) of the line broadening FWHM of tempered martensite caused by rolling contact fatigue.

#### 4.1.8. Cracks within DERs

Subsurface cracks are sometimes found within the DERs, see Figure 23. It is uncertain how and when the cracks are formed. Scott [57] reasoned that the formation of the softer DERs, which is incapable of supporting the stresses imposed, initiates the cracks.

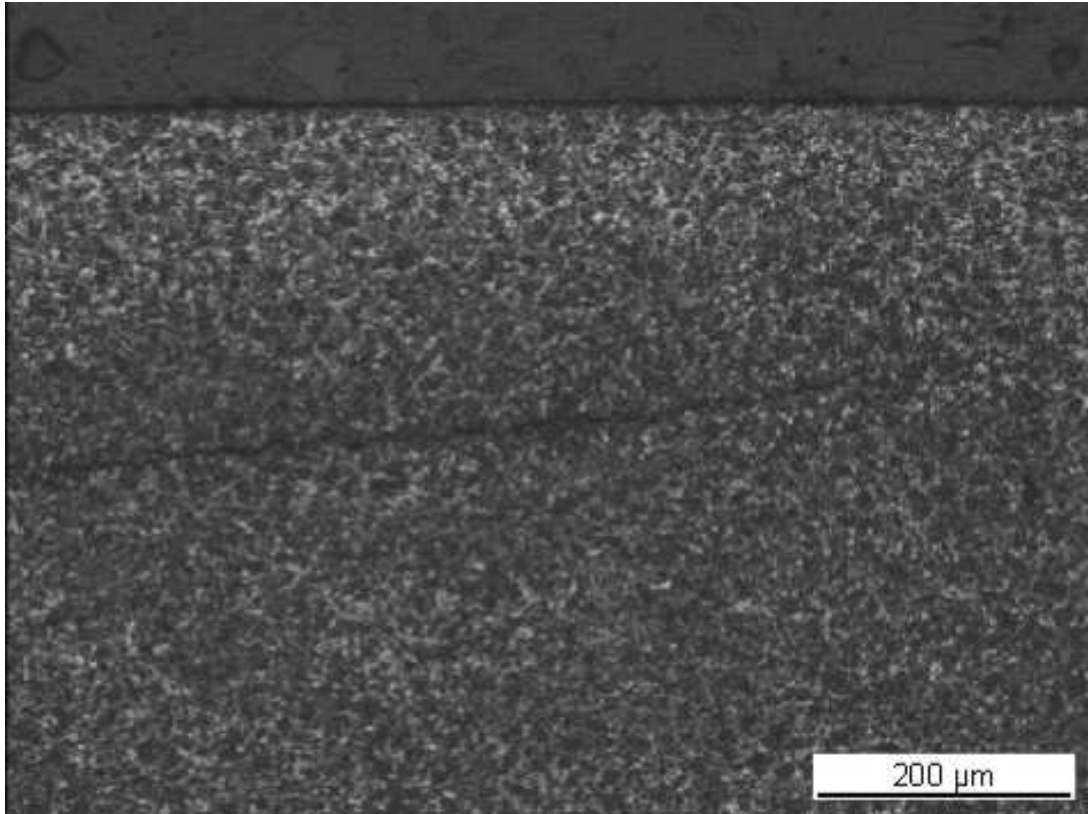


**Figure 23.** Crack observed in the center of the DER in the circumferential (parallel) section. Image from internal SKF work.

#### 4.2. Groove formed on the raceway

A groove with a depth of up to a few micrometres is typically observed on the surface of the raceway of a bearing subjected to RCF. This is a permanent shape change that is due to the plastic deformation caused by the contact with the rolling elements.

In full hydrodynamic lubrication no direct contact between the rolling elements and the raceway is expected. However, full hydrodynamic lubrication cannot be maintained at all times during the bearing lifetime, since below a certain critical sliding velocity there will be a mixed lubrication regime where the thickness of the lubrication film becomes smaller than the size of the surface asperities, resulting in direct contact between the surface of the rolling elements and the raceway. For the above reason, the real area of contact during rolling is limited to the contact between the tips of the asperities, an area significantly smaller than the apparent area calculated by the Hertz theory. This results in very high localised stresses at the contact tips. Some plastic deformation can thus be expected on the tips of the asperities and may result in the breakage of the asperities as well as in the smoothing of the grooved surface.

The formation of the groove decreases the actual contact stress experienced on the subsurface under the same load, due to the increase of the contact area. The severity of the pre-determined contact stress decrease due to the groove formation is dependent on the bearing test, where the ball on flat plate set-up is the most sensitive.

Andersson et al. [44], and Vegter and Slycke [75] have suggested that the formation of the groove on the raceway is a consequence of the sub-surface microstructural changes, or DER formation. Since the formation of the groove can be easily characterised with a profilometer, they have also developed a method based on this idea for assessing the RCF performance of high strength rolling bearing steels. The applicability of this method in relation to DER formation remains to be further popularised.

#### 4.3. X-ray diffraction measurements to map DERs

X-ray powder diffraction (XRD) is a powerful technique and has been used to characterise DERs. It is used to assess the retained-austenite content, texture formation and residual stress build-up after rolling contact fatigue [18]. Voskamp [59] investigated the depth distribution of texture formation, the amount of retained austenite and the residual stresses by electropolishing successive surface layers before X-ray diffraction.

It was observed by Voskamp [18] that the formation of DERs is accompanied by the development of compressive residual stresses and by changes in the FWHM. One example from Voskamp [18] on residual stresses is shown in Figure 24. Residual stresses are measured on samples (cut from (tested) bearings) using standard X-ray diffraction based on the  $\sin 2\Psi$  stress measurement method [18].

The other use of X-ray diffraction analysis is based on the phenomenon of “line-broadening”. In a X-ray diffraction spectrum, each lattice plane is represented by a peak. The stress fields induced by the presence of dislocations displace the atoms from their ideal lattice positions, causing the broadening of the diffraction lines. The analysis of the shape of the peaks indicates the change of dislocation densities.

In addition to the strain broadening caused by dislocations, the diffraction line broadening is also sensitive to the instrumental broadening and the limited size of the crystallites in the specimen, commonly known as size broadening. For a proper interpretation of the diffraction line broadening due to the change of dislocation density, these additional broadening effects need to be taken into account in the analysis. Without these additional considerations, only qualitative estimations of the dislocation

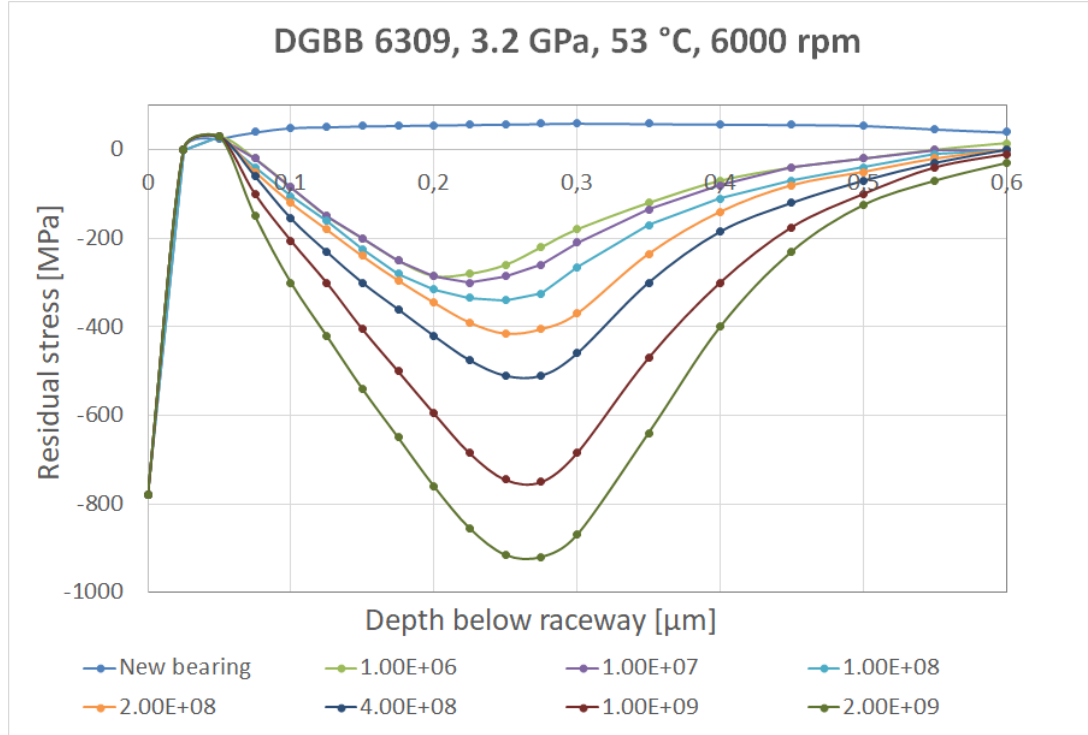


**Figure 24.** Residual stress profiles for DGBB 6309 with martensite hardened inner rings. Adapted from [18].

density can be made.

The qualitative estimation of the dislocation density can be made by the measuring of the “Full Width at Half Maximum” or FWHM of the peak. It can be seen in Figure 25 (schematic figure produced by the authors) that the peak is broad when a material is newly hardened. However the peak becomes sharper in the used bearing.

The decrease of the line-broadening with the appearance of DERs, as seen on Figure 26 indicates the reduction of dislocation density within the DERs. The results presented in the figure were produced by the authors.

#### 4.4. Hardness measurements

The microstructural transformations caused by rolling contact fatigue lead to changes in the mechanical properties of bearings, which are typically characterised by hardness measurements. It seems that the change in hardness during rolling contact fatigue is not of a saturating character, like what is observed in the typical push-pull fatigue tests. Experimental hardness results in the literature show that the changes are irregular, since both hardening or softening can occur depending mainly on the applied contact pressure and operating temperature [14,28]. At the beginning of stress cycling the changes of hardness are relatively small, and their intensity increases with the increasing number of cycles [14,18,28].

While microstructural investigations are typically performed on both cross and parallel sections, hardness measurements are rarely performed on both directions. There are no available reports in the literature on the effect of the sectioning orientation on

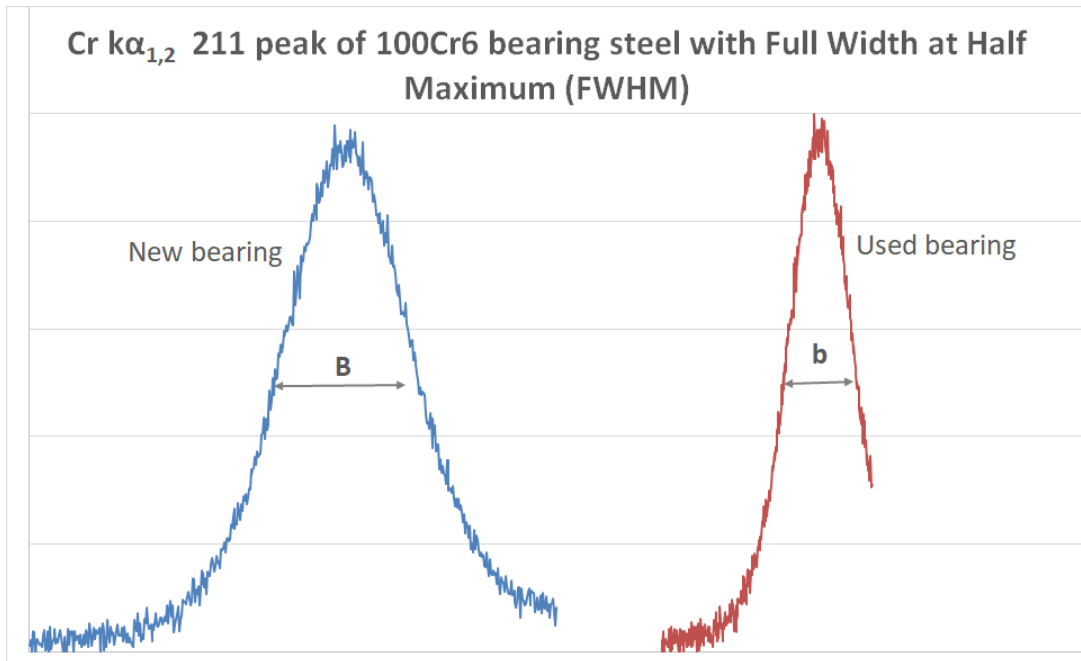


Figure 25. Example of Full Width at Half Maximum of a new and a used bearing.

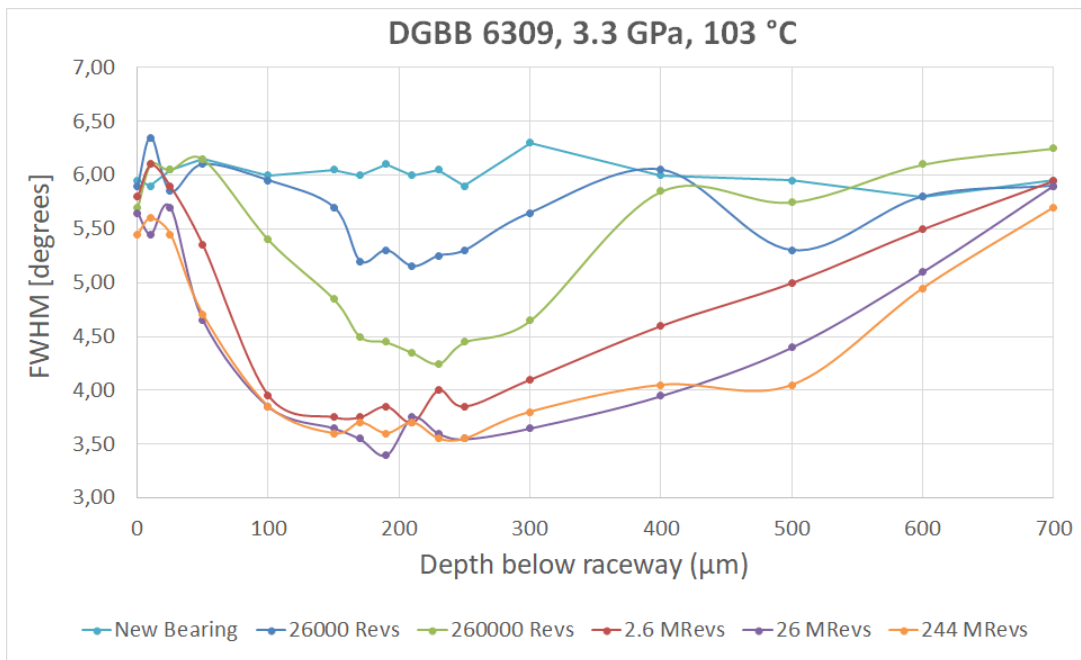
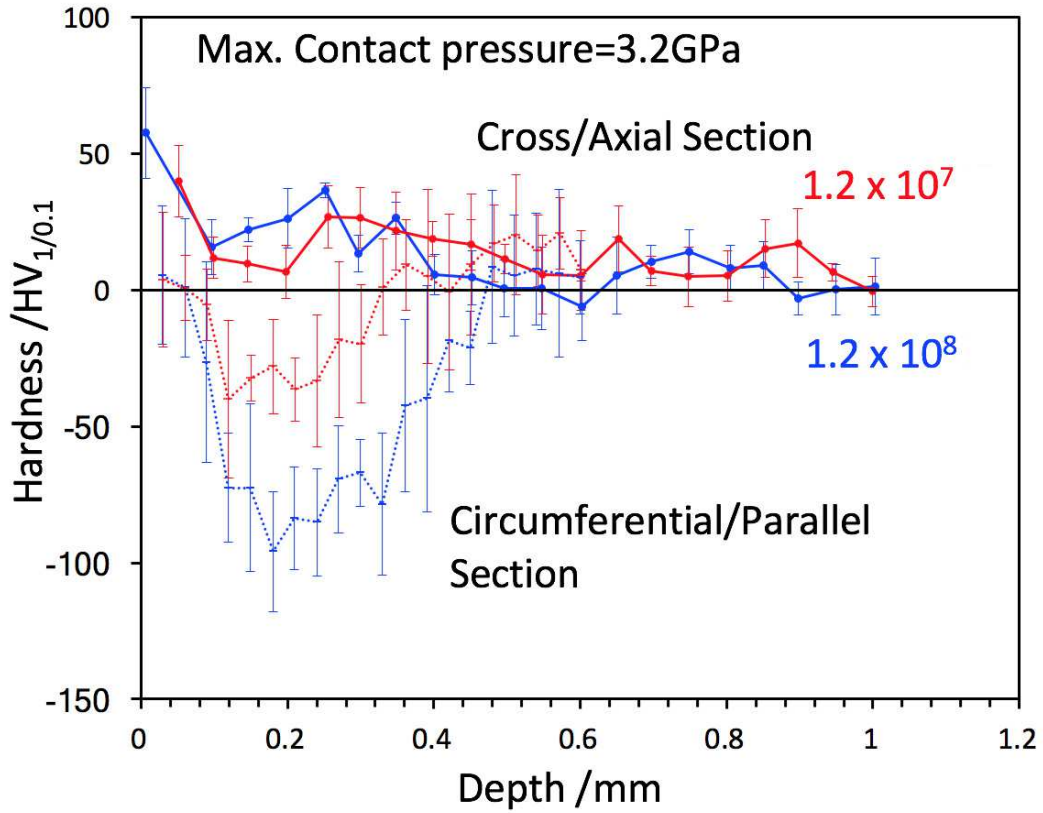


Figure 26. Full Width at Half Maximum profiles for DGBB 6309 with inner ring after martensitic hardening with no retained austenite.

the hardness of the DER, even though DERs have very different microstructures when investigated at different sectioning orientations. Figure 27 shows the DER hardness measurements performed by Kang et al. [62] and Fu et al. [52] on the same bearing but at different sectioning orientations. As can be seen in Figure 27 a small increase of hardness is detected on the cross-section, while a decrease of hardness is measured in the parallel section. The result indicates that the mechanical properties of DERs are anisotropic. Such inconsistency on the hardness results has unintentionally caused confusion on the hardening or softening effect of DERs investigations in the past.



**Figure 27.** Variation of hardness as a function of depth. The measurements were performed in two different sectioning orientations with two different stress cycle Kang et al. [62] and Fu et al. [52]. The dotted line indicates the hardness measurement performed on circumferential(parallel) section sectioning orientation, while the solid line is the hardness measurement on cross-section sectioning orientation. The red and blue colour lines indicate the bearing tested with  $1.2 \times 10^7$  and  $1 \times 10^8$  stress cycles, respectively.

## 5. Mechanisms of formation

The formation of DERs is characterised by the gradual decay of the initial microstructure and is caused by the cyclic Hertzian stresses generated during rolling contact fatigue. As discussed in Section 3.1, the initial microstructure of heat treated bearings includes tempered martensite, tempered carbides, residual cementite and retained austenite. Due to the complexity of the initial multi-phase material, there is still no

consensus in the literature about the fundamental mechanisms of DER formation. Hereby we present some of the theories available in the literature.

### 5.1. Jones [24]

DERs were first observed by Jones in SAE 52100 bearing steel and were described as a structural change that appears in the form of troostite of lower hardness than the original martensite. According to the author, the application of cyclic Hertzian stresses, together with the internal friction of the material, originates the partial transformation of the inflicted shear energy into heat. The accumulation of heat generated due to the cyclic stressing of the material leads to the decay of the hard martensitic phase present in the initial microstructure and the formation of areas of troostite. This phase transformation is the result of subsurface tempering. The authors named their theory the “shear strain energy theory”.

Troostite is an olden term used to name a fine mixture of ferrite and cementite in the 1920s. This mixtures are typically observed in the DERs. Because of the similarity in microstructure, tempering of the parent martensite induced by stress/strain is the main claim in this mechanism to describe the formation of DERs. The necessity for the energy to first transform into heat in order to cause phase transformations, is however questionable.

### 5.2. Bush et al. [31]

Bush et al. studied the nature of the structural changes at the subsurface of ball bearing inner races and rollers subjected to rolling contact fatigue, all of them made from bearing steel SAE 52100. As commonly done, they define the DERs as the area of the material that suffers a more rapid etching attack and, as a result, darkens. They also use the term “stress affected zone” to refer to the DERs, due to the fact that it is initiated in the region of maximum reversed orthogonal shear stress.

In terms of microstructure, they compare the structure of the DERs to that of tempered martensite while showing that in both cases there is a change of the hardness of the microstructure. Nevertheless, they describe it as a zone consisting of extruded carbides and highly deformed ferrite bands. Interestingly, they propose that the augmentation of the coverage of the of DER is a consequence of the nucleation of additional transformed areas, instead of a consequence of the growth of the previously formed dark areas. Additionally, based on the observation that there is a threshold stress for the emergence of DERs, it is suggested that the nucleation of DERs is the result of yielding or a plastic flow phenomenon, instead of a thermal effect.

In terms of the underlying mechanism, they distantiate themselves from Jones’ theory, stating that “heat tempering” is not a condition for the transformation. Instead, they proposed that the transformation is governed by an exchange of material between the carbides and the matrix, a process evidenced by the formation of intrusions/extrusions within the microstructure (see Figure 28).

### 5.3. Swahn et al. [14]

Swahn et al. reported experimental observations on the formation of DERs on SAE 52100 bearing steel, see Figure 29. In their work, the DERs are described as a mixture of 1) a ferritic phase containing inhomogeneously distributed excess carbon, and 2)



**Figure 28.** SAE 52100 steel ball bearing inner race. Transverse section showing intrusions (arrows) and extrusions along edge of undissolved iron carbide particle. Etched in picral [31].

residual martensite from the original microstructure.

The transformation mechanisms that lead to the formation of the new features in the microstructure (DER) are said to be a result of the redistribution of 1) the carbon present in the initial microstructure in solution in martensite, and 2) the carbon resulting from the dissolution of carbides. They also proposed a chronological description of the features that occur during cyclic rolling contact. The main idea is that, initially, stress induced carbon diffusion leads to the migration of carbon from the martensitic lattice towards various defects in the material (mainly dislocations). Then, as plastic deformation accumulates, the movement of dislocations eventually creates carbon rich grain boundary-type interfaces.

Their chronological description of the carbon redistribution in the parent martensite does not incorporate the dissolution of carbides. What the role of carbide dissolution in the formation of the DERs is, and at which timescale carbide dissolution happens within the formation process, are questions that remain unanswered.

#### 5.4. Voskamp [18,59]

Voskamp characterised the DER as decayed martensite, more specifically, as a mixture of martensite and ferrite, the latter resulting from localised, stress-induced phase transformations. The author proposed that stress-induced phase transformations are “not improbable” when the material is subjected to high pulsating loads for a large number of cycles ( $10^8$ – $10^9$ ), a hypothesis that is supported by transmission electron microscope observations of heavily deformed ferritic domains, see Figure 30. The transformations

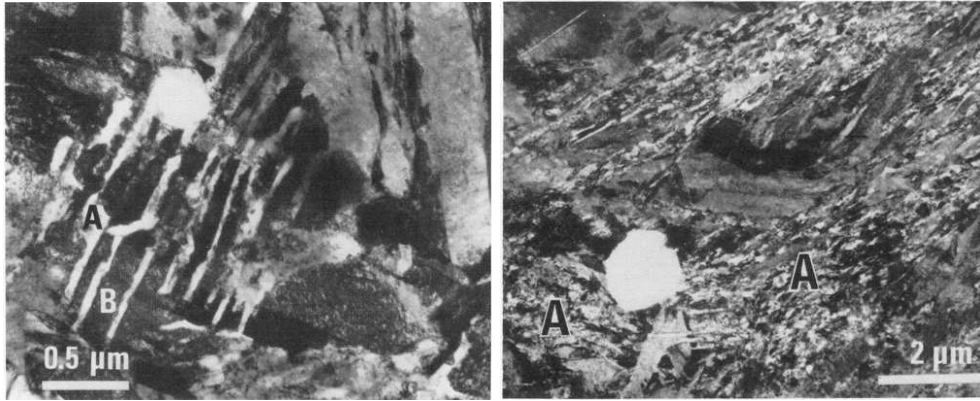


**Figure 29.** Successive stages of the formation of DER on TEM. (Left) Very early stage of martensite decay. A represents transformed zones separated by residual martensite (at B). (Right) Later stage of DER development showing patches where the parent martensite has disappeared [14]

in the microstructure happen in the following order: first, the cyclic stresses generate a local rise in the temperature which induces the diffusion of atomic carbon available in the martensitic matrix. As the carbon diffuses, dislocations that were previously trapped by the carbon are no longer pinned, and potential slip systems are activated. Finally, the movement of the un-pinned dislocations causes plastic deformation.

### 5.5. Polonsky and Keer [35]

Polonsky and Keer proposed a model with the final goal of explaining the phenomenon of white etching band (WEB) formation in rolling bearings. They consider the formation of DERs as a precursory microstructural change to the WEBs, and suggest that both phenomena are the result of the same basic mechanism. Hence, the mechanism that they propose for the formation of the WEBs is also valid to study DERs.

The authors describe the DERs as a region composed of ferritic microbands -regions of localised plastic shear stress- separated by the untransformed parent martensite. The microbands are the result of cyclic-plastic-strain-induced material softening, caused by the redistribution of carbon solute. The driving force for carbon redistribution is ascribed to the stress induced release of atomic carbon into ordinary solution (initially segregated in dislocations).

In more detail, the process is as follows: all dissolved carbon is initially segregated in the form of dislocations atmospheres, due to the high dislocation density of the initial microstructure (martensite); concurrently, the dislocations are pinned by the presence of carbon. When stress is applied, some dislocations are unpinned and become mobile, and a process of dislocation multiplication/annihilation starts. During this process, when a dislocation is annihilated, the carbon atoms in the atmosphere that was previously surrounding it, find themselves in ordinary solution. Hence, the amount of segregated carbon (in dislocations) decreases while the amount of carbon in ordinary solution increases. The carbon in ordinary solution is then available for diffusional flow, resulting in the formation of ferritic microbands, the main characteristic of the microstructural decay inside the DERs.

Additionally, they propose a model to estimate the growth of WEB: it allows to predict the time and number of revolutions required for the formation and growth of

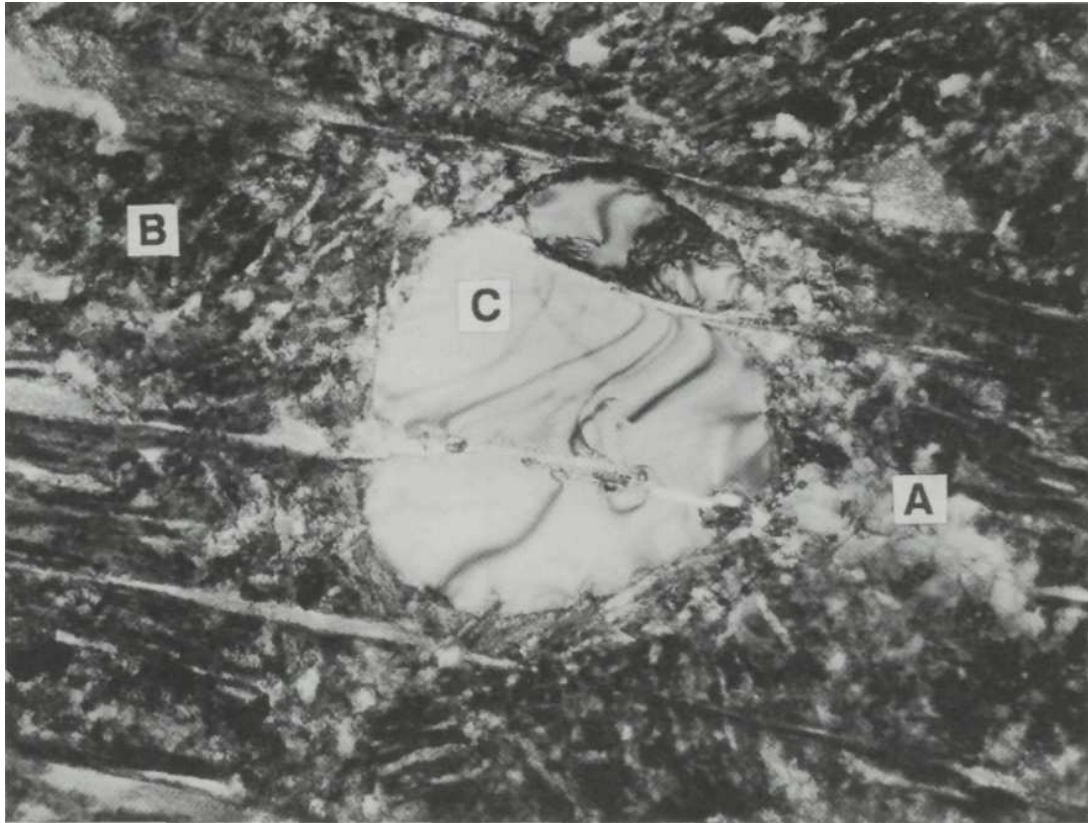


**Figure 30.** TEM image of DER with plasticly deformed ferrite (A), residual martensite (B), and a decaying carbide particle (C) [18].

a fully developed WEB, but not of DERs. Although an extension of this model could be envisioned to predict the formation of DER, it is not yet available in the literature.

### 5.6. *Fu et al.* [52]

Fu et al. describe DERs as a mixture of DER ferrite patches distributed in the parent martensitic matrix. According to the authors, the formation of DERs is strain-induced and it is caused by the orthogonal shear component of the stress inflicted by the Hertzian contact characteristic of rolling. The fundamental mechanism driving the formation of DERs is carbon migration under RCF driven by gliding dislocations. A schematic view of the process of carbon migration is presented in Figure 31. Initially, the material at the surface experiences pulsating stresses as a result of cyclic rolling contact. The strain generated by the pulsating stresses allows the dislocations to escape their atomic-carbon rich environment (Cottrell atmospheres). The now free dislocations behave as places of stress concentration and re-attract the carbon atoms that composed the Cottrell atmospheres that they previously formed. This step-wise motion of dislocations and carbon generates a net carbon flux that ends when the carbon reaches a carbide precipitate (nano-sized tempered carbides).

### 5.7. *Šmeļova et al.* [60]

In a rather recent article, Šmeļova et al. [60] used a variety of characterisation techniques (LOM, SEM, EBSD, EDX, TEM) to study DERs. From LOM observations, they describe DERs as a combination of 1) small black patches intermixed with 2) bright areas and 3) small white primary spheroidised carbides. Residues of 4) retained austenite were also detected using EBSD.

A closer investigation using the Electron Microscope showed that the small black patches correspond to clusters of small globular or elongated ferritic grains (see figure 32), formed during the early stages of the microstructural alterations due to RCF. It is suggested, based on the low misorientation between adjacent grains, the occurrence of high-angle grain boundaries, and their pronounced  $\gamma$ -fibre texture, that the new ferritic grains are the result of recrystallisation processes, possibly dynamic recrystallisation.

The bright areas seen in the LOM correspond to patches of unaltered martensite from the initial microstructure. It was also noticed that the spheroidised (primary/residual) carbides are initially not affected by the decay of the microstructure and are found to be chemically and crystallographically unaltered.

The retained austenite present in the initial microstructure, was partially decomposed and transformed into martensite in the altered region. From their work, it is not clear to what degree has the austenite decomposed and how it is related to the subsequent alterations.

### 5.8. *Summary*

In Table 3 we present a summary of the current section. The different theories to explain the effect of RCF on the decay of the initial microstructure and the changes suffered by each of the individual phases are included.

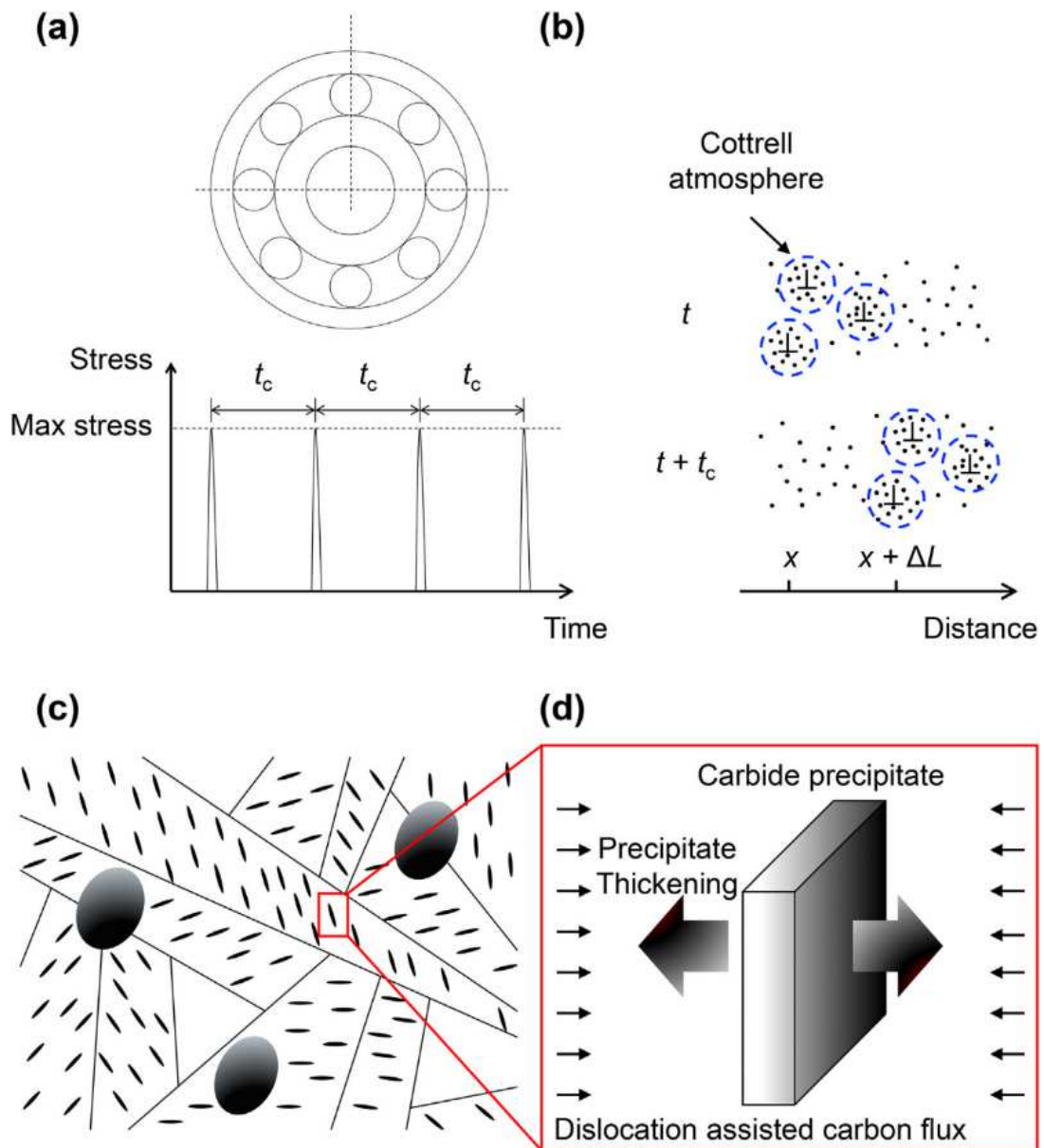


**Figure 31.** Mechanism of dislocation-assisted carbon diffusion during rolling contact fatigue proposed by Fu et al. [52]. a) Stress experienced by the ring of a bearing. b) Cottrell atmospheres dragged by gliding dislocations in a stress cycle. c) Microstructure of tempered martensite. d) Thickening of tempered carbide precipitate.

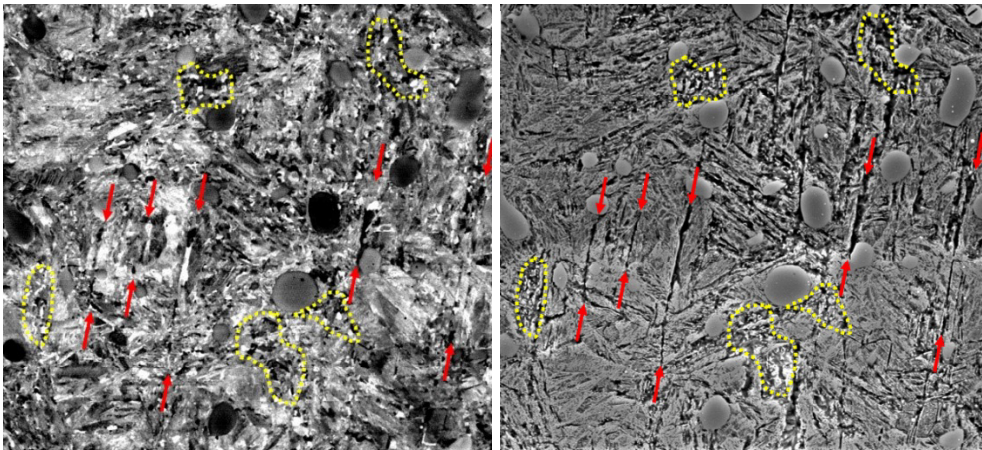


**Figure 32.** Images of DER. (Left) Surface OP-S polished, viewed with backscattered electrons, SEM. (Right) Surface prepared by etching with Nital and viewed with secondary electrons, SEM. Elongated and globular grains are marked with red arrows and yellow dotted lines, respectively [60].

**Table 3.** Evolution of the phases during the formation of DER. Theories found in the literature.

	Smelova et al. Decays	Fu et al. Decays	Voskamp Decays	Swahn Decays	Polonsky and Keer Decays
<b>Martensite</b>					
<b>Retained Austenite</b>	Reduced amount: the retained austenite has been transformed into martensite in the altered region. It can be seen that the amount of retained austenite in the DER is much lower than that in the original microstructure	In this study, the influence of retained austenite is neglected	Three stages can be distinguished in the decomposition of retained Austenite. The first one corresponds with the stage of shakedown. The decomposition is caused by plastic microdeformation. During the second stage, no retained austenite transforms. The third stage is characterised by a drastic decrease of retained austenite with increasing number of inner ring rotations.	There is a considerable martensitic transformation of retained austenite	After a sufficiently large number of revolutions, a complete decomposition of retained austenite in the most stressed subsurface region can occur.
<b>Primary Carbides</b>	The primary spheroidised iron-chromium carbides (Fe,Cr)3C are found to be unaltered within the DER		In association with the development of LABs, the amount of globular cementite in the region of altered microstructure (DER) had become reduced. This is a Stress induced break-up		
<b>Tempered Carbides</b>	Tempered carbides were not detected due to their small size. The study presented in this paper has been primarily performed by use of scanning electron microscopy (SEM, EBSD, EDX). Such tempered carbides could not be observed at this scale	Tempered carbides are initially evenly distributed within a martensitic matrix. The excess carbon in solution migrates to pre-existing (temper) carbide precipitates with the assistance of gliding dislocations, thickening them			
<b>Carbon in Solution</b>			Extensive carbon redistribution is necessary for the observed phase transformations and structural changes, particularly the formation of the large ferrite bands	They assume that the carbon in tempered carbides and in solution in the martensite gradually segregates on dislocations	Diffusionally flows out of DER microbands. There is a redistribution of carbon solute
<b>Chromium</b>	A slightly inhomogeneous chromium distribution in the matrix is also observed, where chromium-depleted regions appear around clusters of primary spheroidised carbides in the matrix.	The Cr content in the DER ferrite is lower than that in the parent martensite, which is probably due to the redistribution of Cr in the vicinity of the Cr-enriched globular carbides. Cr is homogeneously distributed in the DER			
<b>Ferrite</b>	The formation of ferritic globular and elongated grains is observed	DER Ferrite Formed	Heavily deformed ferritic domains are formed. They are the result of a localised, stress-induced phase transformation	RCF generates a ferritic phase, containing an inhomogeneously distributed excess carbon content, corresponding to that of the parent martensite	Carbon outflow from the original microstructure generates DER-ferrite microbands

## 6. Modelling Strategies

### 6.1. Polonsky and Keer [35]

As mentioned in the previous section, Polonsky and Keer propose a model for the formation of white etching bands (WEBs) in rolling bearings. They suggest that the mechanisms that lead to the formation of both WEBs and DERs are the same, and that DERs are precursors of WEBs. Although the model that they propose is not directly applicable to the formation of DERs, we deem it sufficiently relevant to be included in this section.

The model is based on the assumption that WEBs and DERs are regions of localised cyclic plastic shear that form due to plastic deformation and material softening resulting from the redistribution of carbon solute. The driving force for the redistribution of carbon solute (carbon outflow from the WEBs) is assumed to be the release of carbon, initially segregated on dislocations, into ordinary solution.

Let  $C_m$  be the total concentration of dissolved carbon in the martensitic matrix (in wt%). Although  $C_m$  depends on the nominal carbon content in the steel  $C_n$ , the model makes an approximation and assumes these two quantities to be equal.  $C_m$  can be decomposed into the concentration of carbon solute  $C_m^o$  and the average concentration of carbon segregated in the form of dislocation atmospheres  $C_m^a$ :

$$C_m = C_m^o + C_m^a \quad (1)$$

It is also assumed that, initially, all the dissolved carbon is segregated in the form of dislocation atmospheres.

$$C_m^a \approx C_m \text{ and } C_m^o \ll C_m \quad (2)$$

As the material is subjected to cyclic plastic deformation the dislocations start to move, escaping from the carbon atmospheres that surround them. This leads to an intricate process during which dislocations multiply and annihilate, developing a quasi-equilibrium structure. When dislocations are annihilated, the carbon atoms that surrounded them are released and are now in ordinary solution. The result is that, in a given developing band, the concentration of ordinary carbon solution  $C_b^o$  increases while the average concentration of carbon in dislocation atmospheres  $C_b^a$  decreases.

$$C_b^o > C_m^o ; C_b^a < C_m^a \quad (3)$$

This process provides the driving force for carbon outflow from the band, reducing the amount of carbon solute inside it. Simultaneously, the band becomes softer and the dislocation motion within it becomes easier, leading to the formation of the ferrite bands that are seen in DERs (and that will eventually grow to become WEBs). This process, by which the ordinary solute concentration increases per cycle due to the release of segregated carbon, is described by the following equation:

$$\alpha_{to} C_b^a = \alpha_{to} (C_b - C_b^o) \quad (4)$$

where  $\alpha_{to}$  is a dimensionless constant that represents the rate of dislocation turnover (simultaneous multiplication and annihilation) in the band.

The release of segregated carbon is compensated by the concurrent reseggregation of carbon to the dislocations, whose characteristic relaxation time  $t_{rs}$  can be estimated as a function of the coefficient of diffusion of carbon in  $\alpha$ -iron ( $D$ ) and the average spacing between dislocations  $L_d$ , by the following equation:

$$t_{rs} = L_d^2 D^{-1} \quad (5)$$

Assuming that the concentration of ordinary solution in the band is constant during each cycle, the amount of carbon reseggregated per cycle is given by  $C_b^o t_c / t_{rs}$  where,  $t_c$  is the average time between stress cycles. Since the process is in a quasi-equilibrium state, carbon reseggregation is equal to carbon release:

$$C_b^o t_c / t_{rs} = \alpha_{to} (C_b - C_b^o) \quad (6)$$

From the previous equation (Equation [6](#)), it can be deduced that  $C_b^o / C_b \approx 1$ , which means that the dissolved carbon in the band is mostly in ordinary solution –and available for diffusional flow. Since initially the amount of carbon in the band equals the amount of carbon in the matrix ( $C_b = C_m$ ) a rough estimation of the carbon flux is given by:

$$J \approx \frac{D (C_m - C_m^o) \chi}{h} \approx \frac{DC_m \chi}{h} \quad (7)$$

where  $h$  is the thickness of the WEB and  $\chi$  is the density of the material.

Since the total mass of carbon initially contained per unit area of the band is  $C_n \chi h$ , the time  $t_b$  needed for the formation of a fully developed WEB of thickness  $h$  (and, hence, the number of revolutions needed  $N_b$  at a given rotational speed  $n$ ) can be approximated by:

$$t_b \approx \frac{\chi C_n h}{J} \approx \frac{h^2 C_n}{DC_m} \approx \frac{h^2}{D} \quad (8)$$

$$N_b = n t_b \approx \frac{h^2 n}{D} \quad (9)$$

## 6.2. Fu et al. [\[52\]](#)

Fu et al. propose a modelling framework to predict the progress of DER formation and the corresponding evolution of the hardness of the material with increasing number of cycles. The model is based in dislocation assisted carbon migration theory, previously presented in Section [5.6](#)

### 6.2.1. Core of the model

The model starts by the definition or quantification of the dislocation assisted carbon flux ( $J_d$ ) as follows:

$$J_d = \frac{\Delta\gamma\dot{N}}{b} \left[ 3 \left( \frac{\pi}{2} \right)^{\frac{1}{3}} \left( \frac{AD}{k_b T \dot{N}} \right)^{\frac{2}{3}} C_{Vm} \right] \quad (10)$$

where:

$b$	→	Burgers vector
$A$	→	Interaction energy between a carbon atom and a dislocation's strain field
$k_b$	→	Boltzmann constant
$D$	→	Diffusion coefficient of carbon in body centred cubic iron
$T$	→	Temperature
$C_{Vm}$	→	Carbon concentration in the matrix per unit volume
$\Delta\gamma$	→	Plastic shear strain amplitude within each stress cycle
$\dot{N}$	→	Rotational speed

This dislocation assisted carbon flux will contribute to the kinetics of precipitate thickening: the tempered carbides will grow at the expense of the depletion of carbon of the martensitic matrix - that will transform into ferrite.

The second component of the model consist in quantifying the thickening rate of the tempered carbides. Here it is assumed that the tempered carbides are thin plates with a half width of  $r_p$ . The following equation is proposed to maintain equilibrium of the carbon flux. The idea is to equate the carbon flux of precipitate thickening (left side of the equation) with the dislocation assisted carbon migration flux (right side of the equation):

$$\frac{dr_p}{dt} (C_{Vp} - C_{Vm}) = \frac{1}{2} \frac{\Delta\gamma\dot{N}}{b} \left[ 3 \left( \frac{\pi}{2} \right)^{\frac{1}{3}} \left( \frac{AD}{k_b T \dot{N}} \right)^{\frac{2}{3}} C_{Vm} \right] \quad (11)$$

where:

$t$	→	Cycling time
$C_{Vp}$	→	Carbon concentration of the precipitate per unit volume

The third and final part of the model is used to assure that there is carbon mass conservation:

$$l_p C_{V0} = 2r_p C_{Vp} + (l_p - 2r_p) C_{Vm} \quad (12)$$

where:

$l_p$	→	Spacing between precipitates
$C_{V0}$	→	Initial carbon concentration of the system per unit volume

The calculation of DER% is based on the assumption that the decayed martensite (DER ferrite) is completely carbon depleted. This implies that LOM measurements of the fraction of DER ferrite (see Figure 33), are equivalent to the overall extent of carbon depletion in the matrix.

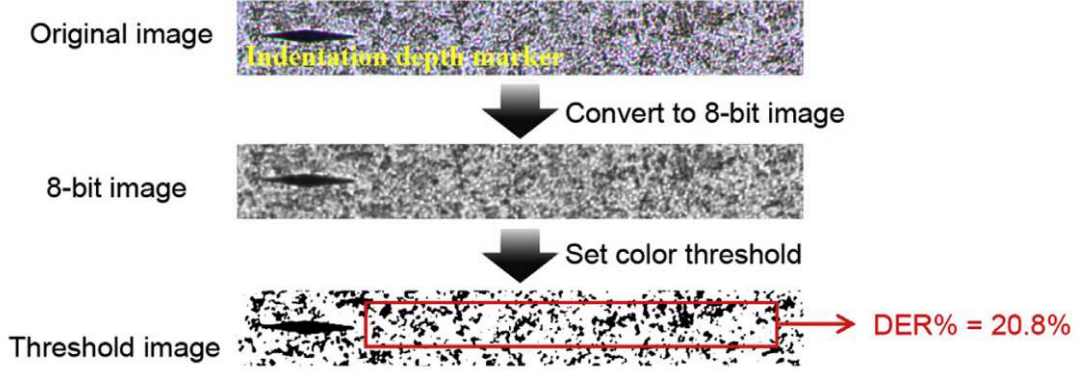


**Figure 33.** Illustration of the method to determine the DER% at a certain depth from optical microscopy used by Fu et al. [52].

Deriving the DER% from the previously explained model requires two steps. First, the evolution of  $C_{Vm}$  is calculated from:

$$C_{Vm} = \frac{l_p C_{V0} - 2r_p C_{Vp}}{l_p - 2r_p} \quad (13)$$

Then, once  $C_{Vm}$  is known, the DER% can be simply calculated as

$$DER\% = \frac{C_{V0} - C_{Vm}}{C_{V0}} \times 100 \quad (14)$$

The calculation of the change in hardness  $\Delta HV$  is based purely on experimental measurements of the hardness of fully formed DERs. The authors assume that there is a linear relationship between the DER% and the change in hardness of the altered microstructure, leading to the following relation:

$$\Delta HV = -150 \times DER\% \quad (15)$$

In a recent article it was claimed that the results of this model represent an over-prediction of the formation of the DERs when compared to experimental data of ball-on-ball RCF tests [20].

Overall, the model predictions are shown to be in a reasonable good agreement with the experiments [52]. However, we note that the diffusion direction of carbon used in Equation [11] is arbitrarily set to go from the matrix towards the temper carbides, since the flux used in the model is always positive (see Equation [10]). The direction of carbon flux in RCF is still part of the heated debate and, as mentioned in Section 4.1.4, further research is needed to clarify this uncertainty. Furthermore, it was found in a recent article that the model predicts faster formation of DERs compared to the experimental data of ball-on-ball RCF tests [20]. It was advocated that a possible reason for the discrepancy comes from the fit for  $\Delta\gamma$  which does not include hardening effects into account. This is very likely to be the case since  $J_d$  depends linearly of  $\Delta\gamma$ , and the maximum contact pressures used in reference [20] are much higher than those used in the original work of Fu et al.

### 6.2.2. Details

**6.2.2.1. Burgers vector ( $b$ ).** In spite of the heterogeneity of the microstructure, a single fixed value for the magnitude of burgers vector ( $b$ ) is used throughout the calculations.

**6.2.2.2. Interaction energy between a carbon atom and a dislocation's strain field  $A$ .** A fixed value is also used for the variable  $A$ , which is called by the authors "interaction energy between a carbon atom and a dislocation's strain field". According to the authors, this constant is taken from [76].

**6.2.2.3. Diffusion coefficient of carbon in body centred cubic iron ( $D$ ).** The diffusion coefficient of carbon is calculated by the model as a function of temperature using the classical equation:

$$D = D_0 \exp(-E/RT) \quad (16)$$

where:

$D_0$	→	Maximal diffusion coefficient for carbon on BCC iron
$E$	→	Activation energy for carbon diffusion on BCC iron
$R$	→	Ideal gas constant

Similarly to what is done with the Burgers vector, it is assumed that the diffusivity of carbon in a specific microstructure (BCC iron) is representative of the diffusivity on the microstructure of bearing steel.

**6.2.2.4. Temperature ( $T$ ) and Rotational Speed ( $\dot{N}$ ).** The temperature considered in the model is the temperate measured during the RCF test, that is, the operational temperature. Similarly,  $\dot{N}$  can also be taken from the test settings.

**6.2.2.5. Carbon concentration per unit volume ( $C_{V0}, C_{Vp}, C_{Vm}$ ).** Perhaps the key element of the model are the three variables that represent the carbon concen-

tration per unit volume in 1) the system as a whole ( $C_{V0}$ ), 2) the tempered carbides ( $C_{Vp}$ ) and 3) the matrix ( $C_{Vm}$ ).

The total carbon content of the system  $C_0$  is taken to be 3.1% from the work of Kang et al. [77] and transformed into  $C_{V0}$  using  $C_{V0} = \frac{2C_0}{a_m^3}$ , where  $a_m$  is the lattice parameter of BCC ferrite.

The carbon concentration of the precipitates, assuming  $\theta$  type carbides (cementite), is calculated via  $C_{Vp} = \frac{4}{a_\theta b_\theta c_\theta}$ , where  $a_\theta, b_\theta, c_\theta$  are the lattice parameters of cementite.

Finally,  $C_{Vm}$  is calculated, as previously explained, using Equation [13]

**6.2.2.6. Plastic shear strain amplitude within each stress cycle ( $\Delta\gamma$ ).** The plastic shear strain amplitude within each stress cycle ( $\Delta\gamma$ ) cannot be directly measured due to the complex stress state typical of rolling contact. To overcome this problem, the authors refer to the work of Hahn et al. [78] who carried out cyclic torsion tests and measured the plastic response of steel to the applied shear stress.

According to the experimental results, ( $\Delta\gamma$ ) increases exponentially with increasing load, and is a function of  $\frac{\tau_a}{\tau_a^{th}} - 1$  (see Figure [34]), where:

$\tau_a$	→	Applied shear stress
$\tau_a^{th}$	→	Threshold shear stress for the onset of plastic response

The threshold for the onset of plastic response is set based on the fact that the depth range of DER formation is 90–500  $\mu\text{m}$ , as shown in the left side of Figure [34].

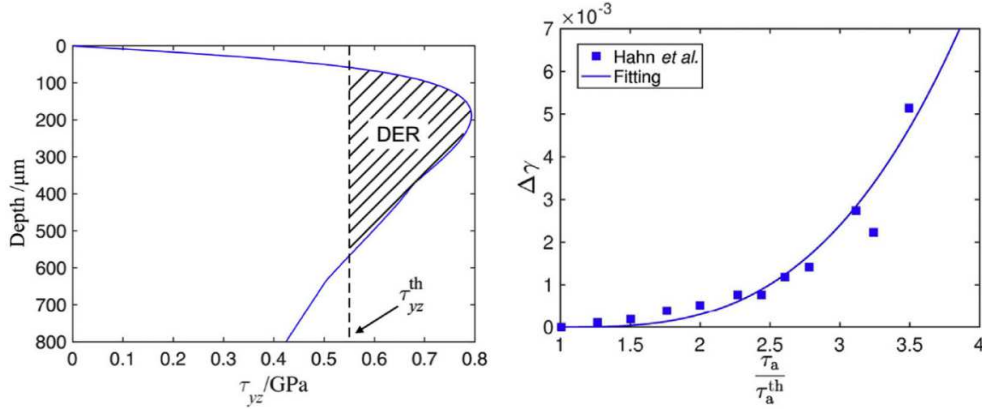


**Figure 34.** (Left) Comparison between the calculated  $\tau_{yz}$  distribution along depth and the observed depth range of DER formation. A threshold  $\tau_{yz}$  for the onset of DER formation is indexed. (Right) Plastic response of the steel determined from the cyclic torsion tests by Hahn et al. [78]. Taken from [52].

The experimental measurements can be fitted to the following equation, which allows the calculation of plastic shear strain amplitude within each stress cycle as a function of the applied shear stress:

$$\Delta\gamma = 0.0003 \left( \frac{\tau_a}{\tau_a^{th}} - 1 \right)^3 \quad (17)$$

The authors then assume that, since the shear stress in rolling contact resultant of

a Hertzian contact pressure  $\tau_{yz}$  is responsible for the generation of DER,  $\tau_a$  can be directly replaced by  $\tau_{yz}$ . Equation 16 can then be written as:

$$\Delta\gamma = 0.0003 \left( \frac{\tau_{yz}}{\tau_{yz}^{th}} - 1 \right)^3 \quad (18)$$

Note that if  $\tau_{yz} < \tau_{yz}^{th}$ , then there is no plasticity and  $\Delta\gamma = 0$

**6.2.2.7. Properties of the precipitates (tempered carbides).** The last elements needed for the model, are the properties of the precipitates. The value of the initial half width of the precipitates  $r_{p0}$  was estimated to be 7 nm, and the initial volume fraction of the precipitates  $f_{p0}$  was estimated to be 6.7 vol%. From these two values, they calculate the spacing between the precipitates to be  $l_p = \frac{2r_{p0}}{f_{p0}}$ .

This modelling approach was independently tested by Abdullah et al. [20] using a modified high-speed microprocessor rotary tribometer where accelerated RCF tests were performed. In their work it was concluded that, for their experiments, the model over-predicts the formation of DERs.

### 6.3. Warhadpande et al. [79]

Similar to the model presented in Section 6.1 the objective of this model is to explain the formation of white etching bands and their orientation. The model is based on the implementation of a stress assisted carbon diffusion equation into a coupled finite element - finite difference framework.

#### 6.3.1. Core of the model

The model uses a stress assisted diffusion law to calculate the flux and the changes in carbon concentration during rolling contact fatigue. The diffusion law is taken from the work of Shewmon [80] who proposes an extension to Fick's law to include the effect of plastic stresses. The carbon flux ( $J$ ) is defined as follows:

$$J = -D \left( \nabla c + \frac{c \nabla V}{kT} \right) \quad (19)$$

where  $c$  is the local concentration of carbon,  $V$  is the plastic dissipated energy,  $k$  is Boltzmann's constant,  $T$  is the temperature (which is assumed to be constant in this work) and  $D$  is the diffusion coefficient.  $D$  is itself related to the activation energy ( $Q$ ) needed for the migration of carbon in  $\alpha$ -ferrite in the following manner:

$$D = D_0 \exp \left( -\frac{Q}{RT} \right) \quad (20)$$

where  $D_0$  is the maximal diffusion coefficient (at infinite temperature) and  $R$  is the universal gas constant. Similarly to what is proposed in Fick's second Law, the

concentration as a function of time  $t$  can be deduced from Equation [21](#):

$$\frac{\partial c}{\partial t} = -D \left( \nabla c + \frac{c \nabla V}{kT} \right) \quad (21)$$

The diffusion of carbon is partially guided by the plastic dissipated energy  $V$ , which is a function of the initial properties of the material and the mechanical constraints applied to the system. The calculation of  $V$  is performed using the finite element model previously developed in [81](#). The model is presented as an elastic-plastic Voronoi finite element (EPVFE) model for rolling contact fatigue of Hertzian line (see Figure [35](#)). It uses Mises based plasticity with linear kinematic hardening.

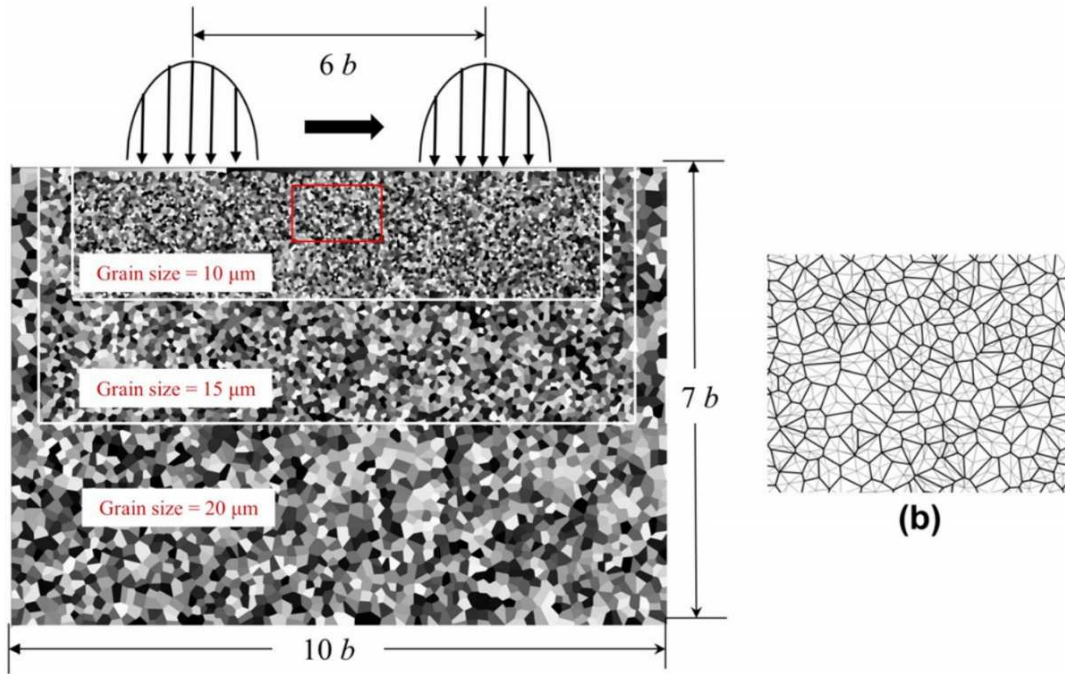


**Figure 35.** Detail of the type of geometry used in the elastic-plastic Voronoi finite element (EPVFE) model for rolling contact fatigue. Figure taken from [81](#).

The diffusion of carbon and, thus, the local changes of carbon concentration, are incorporated in to the EPVFE model using a finite difference scheme. The discretisation of the differential equation determining the concentration (see Equation [21](#)) is performed using an implicit backward Euler equation.

### 6.3.2. Model application

The application of the model is divided into separate, but interlinked, steps that are sequentially repeated for each loading step. The steps are the following:

- (1) Determine the plastic stresses and strains at each element of the domain. This is done by ramping up the applied Hertzian pressure in discrete steps in order to solve the elastic-plastic equations.

- (2) Calculate the dissipated energy due to plastic deformation using the following equation (note that since the model is two dimensional, they use the area ( $A$ ) of the element, and not the volume, for the calculation):

$$V = \left( \int_0^t \sigma_{ij}(\tau) \bullet \varepsilon_{ij}^p(\tau) d\tau \right) A \quad (22)$$

- (3) Solve the diffusion equation and obtain the updated concentrations of carbon. It is important to note that the dependence of the diffusion coefficient on stress is neglected.
- (4) Move the load to a new location.

Additional to the previously mentioned steps, the model incorporates what the authors call a “Jump-in” cycle procedure to accelerate the simulation and cope with the high number of cycles characteristic of rolling contact fatigue in rolling bearings. The main idea is to avoid the re-calculation of the carbon concentration after each step, which can be considerably computationally expensive. For this, the rate of change of carbon concentration is calculated at a given step for all the elements. It is then assumed that for a certain number of cycles, the rate of change of carbon concentration remains constant, which allows to “jump” in time without having to explicitly calculate it at each individual step.

Some comments about the validity of their approach can be made. The motivation for using Equation [22](#) for the calculation of the drift term in the diffusion equation is not clear. There does not seem to be a physical justification for such a choice, and the connection between the dissipated energy due to plasticity and the diffusion of carbon is not clearly explained. Note that the drift term in stress driven diffusion comes from the interaction energy between an external stress field (e.g. crack tip field, dislocation stress field, Hertzian stress, etc.) and the relaxation volume of an interstitial [82](#). A possible explanation is that they wanted to describe the effect of the overall dislocation density on the accelerated diffusion of carbon during RCF. However, such an approach would require a more sophisticated model, perhaps similar to the one developed for hydrogen in [83,84](#). Finally, we also note that the dissipated energy due to plastic deformation is always positive. This entails that its contribution to the diffusion would always point towards the same direction, irrespective of the sign of the externally applied stress. This conflicts with the fact that interstitials with positive relaxation volume are attracted by tensile stresses and repelled by compressive stresses [85](#).

## 7. Discussion

### 7.1. The sequence of events during DER formation

DER formation during rolling contact fatigue is in fact due to the microstructural alterations and subsequent changes to the properties of bearing steels. Reference [18](#) shows the sequence of the microstructural alterations that happen during DER formation (and that will eventually form WEBS and lenticular cementite). The microstructural alterations are the consequence of dislocation rearrangement within the stressed volume. Dislocations move to form elongated ferrite and ferrite microbands. As rolling contact fatigue progresses, the ferrite microbands transform into nanocrystalline ferrite. At the latter stage of rolling contact fatigue, the reduction of the dislocation

density within the grain boundary of nanocrystalline ferrite, diminishes the solubility of carbon; this, in turn promotes the formation of lenticular cementite. Both elongated ferrite and nanocrystalline ferrite form part of the 30° and 80° WEBs. This is in addition to the transformation of retained austenite to martensite at the beginning and the latter stage of rolling contact fatigue.

At a certain stage of the microstructure alteration, the observed microstructure in the DERs has some similarities with the microstructure obtained by severe plastic deformation. Since bearing steel is a relatively brittle material when compared to other engineering materials, fracture can be expected. However, this is usually not the case. The main reasons are that a high hydrostatic component of stress is induced during the rolling contact inhibiting fracture, and the absence of any stress risers. The large plastic strains are the result of incremental strain over the passage of over a billion stress cycles.

### ***7.2. Proposal of a new DER formation mechanism***

The formation of both ferrite microbands and elongated ferrite depends in essence on the dislocation motion and rearrangement, and carbon migration. It is the authors' opinion that the formation of DERs is best understood in terms of the dislocation motion and interaction which accompanies plastic strain, where large plastic strains accumulate during each stress cycle. The observation of the DERs should then be related to the dislocation configurations at a particular number of stress cycles with the added effect of the dissolved carbon. The dislocations can propagate, cross-slip, annihilate, and recombine to form dislocation wall-like and equiaxed cell structures in ferritic steels when experiencing cyclic stress [76,86,87].

The discussions of the formation of these structures are in many cases focused on the dislocation rearrangement into low energy configurations [88]. It has been reported that entangled dislocations rearrange themselves into sub-boundaries with orientations along low-index crystallographic planes (or wall-like structures). Such structures share the same features as the ferrite microbands and the elongated ferrite. The characteristic spacing of these ferrite microbands may be dependent on the applied contact pressure, but further investigation is needed. As rolling contact fatigue progresses, the misorientation across the boundaries increases leading to the formation of equiaxed cell structures (or nanocrystalline ferrite or WEBs in optical microscopy). While we can relate the ferrite microbands and the nanocrystalline ferrite to a simpler fatigue test, at present, there is no theory of elongated ferrite formation. However, it may be related to adiabatic heating during rolling contact [12].

Fundamentally, it is the dislocation interaction with the tempered carbides, the residual cementite and the “dissolved” carbon that will govern the formation of DERs. Both tempered carbides and residual cementite met by the dislocations would be dissolved and removed. The carbon atoms that occupy the dislocation cores (or around strain field/carbon atmospheres) after the dissolution of the carbides would also affect the dislocation movement and its rearrangement. However, there is no attempt to relate the dislocation rearrangement/interactions which occur during cyclic stressing in laboratory setup to rolling contact fatigue in bearings.

A few DER formation mechanisms have been suggested without any concrete microstructural evidence [35,52,79]. Although these models may all contain some elements of the true mechanism(s), dislocation models are thought to have the ability to explain both hardening and softening with the effect of applied contact pressure.

The effectiveness of any model can be judged by two criteria: 1) whether it provides the basis for a quantitative theory of the phenomenon, and 2) whether it suggests experiments to verify its usefulness as a qualitative mean of generalisation to other steels, heat treatment conditions, applied contact pressures, temperatures, number of stress cycles etc.

The importance of dislocation activity (motion, nucleation and annihilation) and its interaction with tempered carbides and residual cementite on the DER formation has been pointed out above. However, our knowledge on this subject is scarce. Work has to be done to further increase the knowledge in this area in order to ultimately be able to model the formation of DERs. In terms of improving bearing life, it seems that the best chance of suppressing DER formation lies in the prevention of dislocation motion and carbon migration in the initial matrix.

## 8. Summary

There are several factors that influence or govern the microstructural alterations in RCF, including the initial structure, residual stresses, and operating conditions, such as contact pressure and temperature. As a thermal-mechanical process, the rate of microstructural alteration increases with contact pressure and / or temperature.

If the maximum contact pressure exceeds a certain limit, the subsurface microstructure below the raceway of a bearing steel undergoes cyclic plasticity. Accumulation of plasticity during rolling contact leads to a microstructural alteration manifested (on nital-etched samples inspected under the light optical microscopy) as a dark-etching region (DER) and, later, as white etching bands (WEBs). Associated with the plastic deformation and the microstructural alterations, the mechanical properties of bearing steels decay progressively, leading eventually to subsurface initiated fatigue failure in the form of raceway spalling.

The alteration of the microstructure is a process of carbon migration driven by dislocation rearrangement, summarised in Figure 36 by the authors. For bearing steels with martensitic hardening, the initial structure consists of tempered martensite containing nano-sized precipitates (transition carbides), retained austenite (RA) and residual cementite (RC). Formation of DERs involves the transformation of tempered martensite to ferrite in the form of ferrite microbands and elongated ferrite, as a result of dislocation driven carbon migration from the martensitic matrix. In the meantime, RA transforms partially to martensite as a result of stress- and strain-induced phase transformations, while the residual carbides are intact at early stage but are gradually dissolved in some regions of highly localised plasticity. With the progression of RCF, the ferrite microbands and the elongated ferrite grains develop further to become ferrite bands that are visualised as low-angle-bands (LABs) and high-angle-bands (HABs). The carbon atoms from the matrix and dissolved carbides segregate to form lenticular carbides at the edge of the ferrite bands.

There exists still dispute regarding the destination of carbon migration at the stage of DER formation. The specific question is if the carbon atoms inside martensite are transported towards the transition carbides, causing the so-called carbide coarsening, or to somewhere else such as the boundaries of the newly formed ferrite microbands or elongated ferrite grains.

Microstructure decay during RCF is also reflected in the change of the mechanical properties of the material. At the early stage of RCF, hardness increases as a result of work hardening. With the progression of RCF, the dislocation driven carbon migration

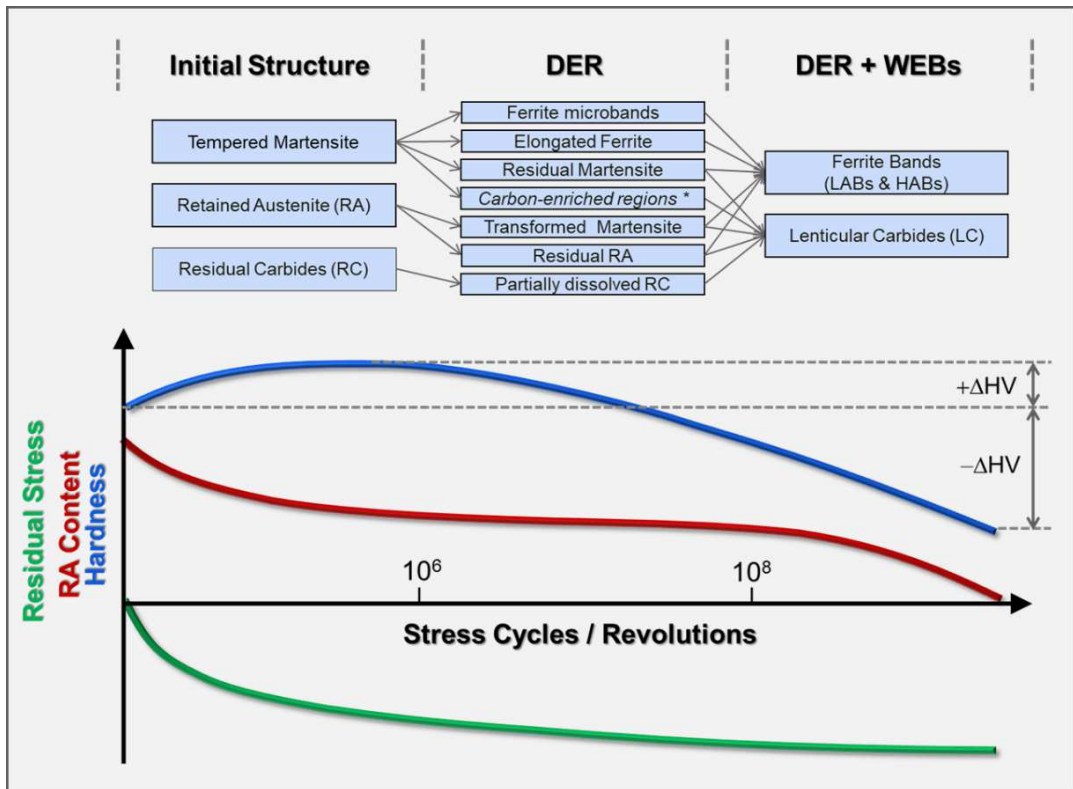


**Figure 36.** A map of bearing steel microstructure alterations and the associated change of properties, visualised for a martensitic structure.

leads to increasingly inhomogeneous / decayed microstructure characterised by carbon depleted regions mixed with carbon enriched regions. The carbon depletion of the martensitic matrix causes gradual decrease in hardness of the decayed microstructure.

Cyclic stress and strain in the subsurface region leads to the decomposition of Retained Austenite (RA). At advanced stages of RCF, the decomposition of RA tends to be complete and the RA content decreases to zero. Associated with the accumulation of plasticity and phase transformation, compressive residual stresses are built up in the subsurface region.

Compared to the extensive experimental study and characterisation of bearing steel microstructural alterations in RCF, the work to model such material degradation is so far rather limited. Since recently, there have been a few papers published in the literature that make an effort to model the carbon diffusion and migration associated with the microstructural alterations of bearing steels under RCF. However, there still exists a gap between the observed features of the microstructural alterations and the predictions of the models.

Most investigations so far focus on the martensitic structure of AISI 52100 (Grade 3) steel. Material degradation of other microstructures and steel alloys in RCF remains to be investigated in the future.

## Acknowledgement(s)

SWO was a Deputy Director at SKF, University Technology Center at the University of Cambridge when the majority of this work was carried out. SWO is grateful to Professor Sir Harry Bhadeshia for helpful discussions. The authors would like to thank Guillermo E. Morales-Espejel, Mohamed Sherif and Marica Ersson for their critical review of the manuscript.

## References

- [1] Brizmer V, Gabelli A, Vieillard C, et al. An Experimental and Theoretical Study of Hybrid Bearing Micropitting Performance under Reduced Lubrication. *Tribology Transactions*. 2015 sep;58(5):829–835. Available from: <http://www.tandfonline.com/doi/full/10.1080/10402004.2015.1021944>
- [2] Brizmer V, Stadler K, van Drogen M, et al. The Tribological Performance of Black Oxide Coating in Rolling/Sliding Contacts. *Tribology Transactions*. 2017 may;60(3):557–574. Available from: <http://dx.doi.org/10.1080/10402004.2016.1186258><https://www.tandfonline.com/doi/full/10.1080/10402004.2016.1186258>
- [3] Brizmer V, Matta C, Nedelcu I, et al. The Influence of Tribolayer Formation on Tribological Performance of Rolling/Sliding Contacts. *Tribology Letters*. 2017 jun;65(2):57. Available from: <http://link.springer.com/10.1007/s11249-017-0839-3>
- [4] Vieillard C, Kadin Y, Morales-Espejel G, et al. An experimental and theoretical study of surface rolling contact fatigue damage progression in hybrid bearings with artificial dents. *Wear*. 2016 oct;364-365:211–223. Available from: <http://dx.doi.org/10.1016/j.wear.2016.07.016><https://linkinghub.elsevier.com/retrieve/pii/S0043164816301582>
- [5] Morales-Espejel GE, Brizmer V. Micropitting Modelling in Rolling–Sliding Contacts: Application to Rolling Bearings. *Tribology Transactions*. 2011 jul;54(4):625–643. Available from: <http://www.tandfonline.com/doi/abs/10.1080/10402004.2011.587633>
- [6] Brizmer V, Pasaribu HR, Morales-Espejel GE. Micropitting Performance of Oil Additives in Lubricated Rolling Contacts. *Tribology Transactions*. 2013 sep;56(5):739–

748. Available from: <http://dx.doi.org/10.1080/10402004.2013.790097><http://www.tandfonline.com/doi/full/10.1080/10402004.2013.790097>
- [7] POPESCU G, MORALES-ESPEJEL GE, WEMEKAMP B, et al. An Engineering Model for Three-Dimensional Elastic-Plastic Rolling Contact Analyses. *Tribology Transactions*. 2006 sep;49(3):387–399. Available from: <http://www.tandfonline.com/doi/abs/10.1080/05698190600678739>.
  - [8] Vegter RH, Slycke JT, Beswick J, et al. The Role of Hydrogen on Rolling Contact Fatigue Response of Rolling Element Bearings. *Journal of ASTM International*. 2010;7(2):102543. Available from: <http://www.astm.org/doiLink.cgi?JAI102543>.
  - [9] Merwin JE, Johnson KL. An Analysis of Plastic Deformation in Rolling Contact. *Proceedings of the Institution of Mechanical Engineers*. 1963 jun; 177(1):676–690. Available from: [http://journals.sagepub.com/doi/10.1243/PIME{}\\_PROC{}\\_1963{}\\_177{}\\_052{}\\_02](http://journals.sagepub.com/doi/10.1243/PIME{}_PROC{}_1963{}_177{}_052{}_02)
  - [10] Bhadeshia H. Steels for bearings. *Progress in Materials Science*. 2012 feb;57(2):268–435. Available from: <http://dx.doi.org/10.1016/j.pmatsci.2011.06.002><http://linkinghub.elsevier.com/retrieve/pii/S0079642511000922>.
  - [11] El Laithy M, Wang L, Harvey TJ, et al. Further understanding of rolling contact fatigue in rolling element bearings - A review. *Tribology International*. 2019 dec;140(April):105849. Available from: <https://doi.org/10.1016/j.triboint.2019.105849><https://linkinghub.elsevier.com/retrieve/pii/S0301679X19303561>.
  - [12] Ooi SW, Gola A, Vegter RH, et al. Evolution of white-etching cracks and associated microstructural alterations during bearing tests. *Materials Science and Technology (United Kingdom)*. 2017;33(14):1657–1666. Available from: <http://dx.doi.org/10.1080/02670836.2017.1310431>
  - [13] Lai J, Stadler K. Investigation on the mechanisms of white etching crack (WEC) formation in rolling contact fatigue and identification of a root cause for bearing premature failure. *Wear*. 2016 oct;364-365:244–256. Available from: <https://linkinghub.elsevier.com/retrieve/pii/S0043164816301636>
  - [14] Swahn H, Becker PC, Vingsbo O. Martensite decay during rolling contact fatigue in ball bearings. *Metallurgical Transactions A*. 1976 aug;7(8):1099–1110. Available from: <http://link.springer.com/10.1007/BF02656592>
  - [15] Schlicht H, Schreiber E, Zwirlein O. Effects of Material Properties on Bearing Steel Fatigue Strength. In: *Effect of steel manufacturing processes on the quality of bearing steels*. 100 Barr Harbor Drive, PO Box C700, West Conshohocken, PA 19428-2959: ASTM International; 1988. p. 81–81–21. Available from: <http://www.astm.org/doiLink.cgi?STP26228S>
  - [16] Warhadpande A, Sadeghi F, Evans RD. Microstructural Alterations in Bearing Steels under Rolling Contact Fatigue Part 1—Historical Overview. *Tribology Transactions*. 2013 may;56(3):349–358. Available from: <http://www.tandfonline.com/doi/abs/10.1080/10402004.2012.754073>
  - [17] Gabelli A, Morales-Espejel GE. A model for hybrid bearing life with surface and subsurface survival. *Wear*. 2019 mar;422-423(January):223–234. Available from: <https://doi.org/10.1016/j.wear.2019.01.050><https://linkinghub.elsevier.com/retrieve/pii/S0043164818312894>
  - [18] Voskamp AP. Microstructural changes during rolling rolling contact fatigue Doctoral thesis. Delft University of Technology; 1997. Available from: <http://resolver.tudelft.nl/uuid:783a0a39-6062-4326-b493-a4dee0efef92>
  - [19] Vasilca G, Raszillier V. A study of dark etching area (D.E.A.) type structure modification of material and hertzian contact area induced by ball bearing type motion. *Wear*. 1972; 19(1):1–15.
  - [20] Abdullah MU, Khan ZA, Kruhoeffler W. Evaluation of Dark Etching Regions for Standard Bearing Steel under Accelerated Rolling Contact Fatigue. *Tribology International*. 2020 dec;152:106579. Available from: <https://doi.org/10.1016/j.triboint.2020.106579><https://linkinghub.elsevier.com/retrieve/pii/S0301679X20304096>

- [21] Lundberg G, Palmgren A. Dynamic capacity of rolling bearings. *Acta Polytechnica - Mechanical Engineering Series*. 1947;1:4–51.
- [22] Dieter G. *Mechanical Metallurgy*. Boston, MA: McGraw-Hill; 1986.
- [23] Carter TL, Zaretsky EV, Anderson WJ. Effect of hardness and other mechanical properties on rolling–contact fatigue life of four high–temperature bearing steels. Cleveland: National Aeronautics and Space Administration; 1960. NASA-TN-D-270.
- [24] Jones AB. Metallographic Observations of Ball Bearing Fatigue Phenomena. In: Symposium on testing of bearings. 100 Barr Harbor Drive, PO Box C700, West Conshohocken, PA 19428-2959: ASTM International; 1946. p. 35–35–18. Available from: <http://www.astm.org/doiLink.cgi?STP42598S>
- [25] Swahn H, Becker PC, Vingsbo O. Electron-microscope studies of carbide decay during contact fatigue in ball bearings. *Metal Science*. 1976 jan;10(1):35–39. Available from: <http://www.tandfonline.com/doi/full/10.1179/030634576790431444>
- [26] Osterlund R, Vingsbo O. Phase changes in fatigued ball bearings. *Metallurgical Transactions A*. 1980 may;11(5):701–707. Available from: <http://link.springer.com/10.1007/BF02661199>
- [27] Becker PC, Swahn H, Vingsbo O. Structural changes in ball bearing steels caused by rolling contact fatigue. *Mechanique matériaux électricité*. 1976;320-321:8–14.
- [28] Kuroda M. On the Mechanism of Flaking Due to Rolling Fatigue of Ball and Roller Bearing Steels. *Transactions of the Japan Society of Mechanical Engineers*. 1960;26(169):1258–1271. Available from: [https://www.jstage.jst.go.jp/article/cpb1958/33/4/33\\_{ }4\\_{ }1660/{ }articlehttp://joi.jlc.jst.go.jp/JST.Journalarchive/kikai1938/26.1258?from=CrossRef](https://www.jstage.jst.go.jp/article/cpb1958/33/4/33_{ }4_{ }1660/{ }articlehttp://joi.jlc.jst.go.jp/JST.Journalarchive/kikai1938/26.1258?from=CrossRef)
- [29] Muro H, Tsushima N. Microstructural, microhardness and residual stress changes due to rolling contact. *Wear*. 1970 may;15(5):309–330. Available from: <http://linkinghub.elsevier.com/retrieve/pii/0043164870901766http://joi.jlc.jst.go.jp/JST.Journalarchive/kikai1938/26.1258?from=CrossRef>
- [30] Tunca N, Laufer EE. Wear mechanisms and finite element crack propagation analysis of high speed roller bearings. *Wear*. 1987;118(1):77–97.
- [31] Bush JJ, Grube WL, Robinson GH. Microstructural and residual stress changes in hardened steel due to rolling contact. *Trans Amer Soc Metals*. 1961;54:390–412,818–823.
- [32] Martin JA, Borgese SF, Eberhardt AD. Microstructural Alterations of Rolling—Bearing Steel Undergoing Cyclic Stressing. *Journal of Basic Engineering*. 1966;88(3):555. Available from: <http://fluidsengineering.asmedigitalcollection.asme.org/article.aspx?articleid=1432755>
- [33] SHIBATA M, LEE H. Long Life Bearing Made of Greater Toughness Bearing Steel. *Koyo Engineering Journal*. 1992;(141):26–30.
- [34] Hyde RS. Contact Fatigue of Hardened Steels. In: *Fatigue and fracture*. ASM International; 1996. p. 691–703. Available from: <https://dl.asminternational.org/books/book/34/chapter/459507/contact-fatigue-of-hardened-steels>
- [35] Polonsky I, Keer LM. On white etching band formation in rolling bearings. *Journal of the Mechanics and Physics of Solids*. 1995 apr;43(4):637–669. Available from: <http://linkinghub.elsevier.com/retrieve/pii/002250969500001Yhttps://linkinghub.elsevier.com/retrieve/pii/002250969500001Y>
- [36] Barrow A, Rivera-Díaz-del Castillo P. Nanoprecipitation in bearing steels. *Acta Materialia*. 2011 nov;59(19):7155–7167. Available from: <https://linkinghub.elsevier.com/retrieve/pii/S135964541100574X>
- [37] Zhukov V, Gubanov V, Jarlborg T. Study of energy-band structures, some thermomechanical properties and chemical bonding for a number of refractory metal carbides by the LMTO-ASA method. *Journal of Physics and Chemistry of Solids*. 1985 jan; 46(10):1111–1116. Available from: <http://linkinghub.elsevier.com/retrieve/pii/0022369785901398>
- [38] Yajima E, Miyazaki T, Sugiyama T, et al. Effects of Retained Austenite on the Rolling Fatigue Life of Ball Bearing Steels. *Trans Jap Inst Met*. 1974;15(3):173–179.

- [39] Tricot R, Monnot J, Lluansi M. How microstructural alterations affect fatigue properties of 52100 steel. *Metals Engineering Quarterly*. 1972;12:39–47.
- [40] Shiko S, Okamoto K, Watanabe S. Effect of Metallographical Factors on the Rolling Fatigue Life of Ball Bearing Steel. *Tetsu-to-Hagane*. 1968;54(13):1353–1366. Available from: [https://www.jstage.jst.go.jp/article/tetsutohagane1955/54/13/54\\_{\\_}13\\_{\\_}1353/{\\_}article/-char/ja/](https://www.jstage.jst.go.jp/article/tetsutohagane1955/54/13/54_{_}13_{_}1353/{_}article/-char/ja/)
- [41] Aoki K, Nagumo M, Sugino K. Some Metallurgical Problems on the Life of Rolling Bearing. *Nippon Steel*; 1973. 2.
- [42] Bhadeshia HKDH, Honeycombe R. *Steels: Microstructure and Properties*. Elsevier; 2006. Available from: <https://linkinghub.elsevier.com/retrieve/pii/B9780750680844X50006>.
- [43] Leslie W, Hornbogen E. Physical metallurgy of steels. In: *Physical metallurgy*. Elsevier; 1996. p. 1555–1620. Available from: <https://linkinghub.elsevier.com/retrieve/pii/B9780444898753500223>.
- [44] Andersson JE, Wicks G, Olund PLJ. Raceway Grooving: A Tool for Monitoring Microstructural Changes. In: *Bearing steel technologies: 9th volume, advances in rolling contact fatigue strength testing and related substitute technologies*. 100 Barr Harbor Drive, PO Box C700, West Conshohocken, PA 19428-2959: ASTM International; 2012. p. 291–302. Available from: <http://www.astm.org/doiLink.cgi?STP104643>.
- [45] Ande CK, Sluiter MH. First-principles prediction of partitioning of alloying elements between cementite and ferrite. *Acta Materialia*. 2010 nov;58(19):6276–6281. Available from: <http://linkinghub.elsevier.com/retrieve/pii/S1359645410004933>.
- [46] Simonovic D, Ande CK, Duff AI, et al. Diffusion of carbon in bcc Fe in the presence of Si. *Physical Review B*. 2010 feb;81(5):054116. Available from: <https://link.aps.org/doi/10.1103/PhysRevB.81.054116>
- [47] Bhadeshia HKDH, Solano-Alvarez W. Critical Assessment 13: Elimination of white etching matter in bearing steels. *Materials Science and Technology*. 2015 jul; 31(9):1011–1015. Available from: <http://www.tandfonline.com/doi/full/10.1179/1743284715Y.0000000036>.
- [48] Mitamura N, Hidaka H, Takaki S. Microstructural Development in Bearing Steel during Rolling Contact Fatigue. *Materials Science Forum*. 2007 mar;539-543:4255–4260. Available from: <http://www.scientific.net/MSF.539-543.4255https://www.scientific.net/MSF.539-543.4255>.
- [49] Lund T. Structural Alterations in Fatigue-Tested Ball-Bearing Steel. *Jernkontorets Annaler*. 1969;153(7):337–343.
- [50] Mughbrabi H, Ackermann F, Herz K. Persistent Slipbands in Fatigued Face-Centered and Body-Centered Cubic Metals. In: *Fatigue mechanisms*. 100 Barr Harbor Drive, PO Box C700, West Conshohocken, PA 19428-2959: ASTM International; 1979. p. 69–69–37. Available from: <http://www.astm.org/doiLink.cgi?STP35885S>.
- [51] Fu H. *Microstructural alterations in bearing steels under rolling contact fatigue* Doctoral thesis. University of Cambridge; 2017. Available from: <https://www.repository.cam.ac.uk/handle/1810/270311>.
- [52] Fu H, Song W, Galindo-Nava EI, et al. Strain-induced martensite decay in bearing steels under rolling contact fatigue: Modelling and atomic-scale characterisation. *Acta Materialia*. 2017 oct;139:163–173. Available from: <http://dx.doi.org/10.1016/j.actamat.2017.08.005http://linkinghub.elsevier.com/retrieve/pii/S1359645417306481>.
- [53] Smeļova V, Schwedt A, Wang L, et al. Microstructural changes in White Etching Cracks (WECs) and their relationship with those in Dark Etching Region (DER) and White Etching Bands (WEBs) due to Rolling Contact Fatigue (RCF). *International Journal of Fatigue*. 2017 jul;100:148–158. Available from: <http://linkinghub.elsevier.com/retrieve/pii/S014211231730141X>
- [54] King AH, O’Brien JL. Microstructural Alterations in Rolling Contact Fatigue. In: *Advances in electron metallography: Vol. 6*. 100 Barr Harbor Drive, PO Box C700, West Conshohocken, PA 19428-2959: ASTM International; 1965. p. 74–74–15. Available from:

- <http://www.astm.org/doiLink.cgi?STP46420S>.
- [55] Scott D, Blackwell J. Paper 17: Study of Sintered Carbides and Surface-Treated Materials for Unlubricated and Elevated Temperature Rolling Elements. Proceedings of the Institution of Mechanical Engineers, Conference Proceedings. 1966 jun;181(15):77–84. Available from: <http://journals.sagepub.com/doi/10.1243/PIME{ }CONF{ }1966{ }181{ }301{ }02>
- [56] Turkalo AM. An Electron Transmission Study of the Tempering of Martensite in a 0.42% Carbon Steel. Transactions of the ASM. 1961;54:344.
- [57] Scott D. Rolling Contact Fatigue. In: Structural integrity. Vol. 9. ACADEMIC PRESS, INC.; 1979. p. 321–361. Available from: [http://dx.doi.org/10.1016/S0161-9160\(13\)70072-3https://linkinghub.elsevier.com/retrieve/pii/S0161916013700723](http://dx.doi.org/10.1016/S0161-9160(13)70072-3https://linkinghub.elsevier.com/retrieve/pii/S0161916013700723)
- [58] HARADA H, MIKAMI T, SHIBATA M, et al. Microstructural Changes and Crack Initiation with White Etching Area Formation under Rolling/Sliding Contact in Bearing Steel. ISIJ International. 2005;45(12):1897–1902. Available from: <http://joi.jlc.jst.go.jp/JST.JSTAGE/isijinternational/45.1897?from=CrossRef>
- [59] Voskamp AP, Osterlund R, Becker PC, et al. Gradual changes in residual stress and microstructure during contact fatigue in ball bearings. Metals Technology. 1980 jan;7(1):14–21. Available from: <http://www.tandfonline.com/doi/full/10.1179/030716980803286676>
- [60] Šmeļova V, Schwedt A, Wang L, et al. Electron microscopy investigations of microstructural alterations due to classical Rolling Contact Fatigue (RCF) in martensitic AISI 52100 bearing steel. International Journal of Fatigue. 2017 may;98:142–154. Available from: <http://linkinghub.elsevier.com/retrieve/pii/S0142112317300427>
- [61] Borgese S. An Electron Fractographic Study of Spalls Formed in Rolling Contact. Journal of Basic Engineering. 1967 dec;89(4):943–948. Available from: <https://asmedigitalcollection.asme.org/fluidsengineering/article/89/4/943/397915/An-Electron-Fractographic-Study-of-Spalls-Formed>
- [62] Kang J. Mechanisms of microstructural damage during rolling contact fatigue of bearing steels [dissertation]. University of Cambridge; 2014. Available from: <https://www.repository.cam.ac.uk/handle/1810/245255>
- [63] Christian JW. Tetragonal Martensites in Ferrous Alloys &mdash; A Critique. Materials Transactions, JIM. 1992;33(3):208–214. Available from: <https://www.jstage.jst.go.jp/article/matertrans1989/33/3/33{ }3{ }208/{ }article>
- [64] Voskamp AP. Material Response to Rolling Contact Loading. Journal of Tribology. 1985 jul;107(3):359–364. Available from: <https://asmedigitalcollection.asme.org/tribology/article/107/3/359/437484/Material-Response-to-Rolling-Contact-Loading>
- [65] Hahn GT, Bhargava V, Rubin CA, et al. Analysis of the Rolling Contact Residual Stresses and Cyclic Plastic Deformation of SAE 52100 Steel Ball Bearings. Journal of Tribology. 1987 oct;109(4):618–626. Available from: <https://asmedigitalcollection.asme.org/tribology/article/109/4/618/433650/Analysis-of-the-Rolling-Contact-Residual-Stresses>
- [66] Christian JW. Crystallographic theories, interface structures, and transformation mechanisms. Metallurgical and Materials Transactions A. 1994 sep;25(9):1821–1839. Available from: <http://link.springer.com/10.1007/BF02649031>
- [67] Keh A. Imperfections and plastic deformation of cementite in steel. Acta Metallurgica. 1963 sep;11(9):1101–1103. Available from: <https://linkinghub.elsevier.com/retrieve/pii/0001616063902013>
- [68] Nematollahi GA, Grabowski B, Raabe D, et al. Multiscale description of carbon-supersaturated ferrite in severely drawn pearlitic wires. Acta Materialia. 2016 jun;111:321–334. Available from: <https://linkinghub.elsevier.com/retrieve/pii/S1359645416302051>
- [69] Languillaume J, Kapelski G, Baudalet B. Cementite dissolution in heavily cold drawn pearlitic steel wires. Acta Materialia. 1997 mar;45(3):1201–1212. Available from: <https://>

- 
- [//linkinghub.elsevier.com/retrieve/pii/S1359645496002169](http://linkinghub.elsevier.com/retrieve/pii/S1359645496002169)
- [70] Hong MH, Reynolds WT, Tarui T, et al. Atom probe and transmission electron microscopy investigations of heavily drawn pearlitic steel wire. *Metallurgical and Materials Transactions A*. 1999 mar;30(13):717–727. Available from: <http://link.springer.com/10.1007/s11661-999-1003-y>.
- [71] McGrath JT, Bratina WJ. Dislocation structures in fatigued iron-carbon alloys. *Philosophical Magazine*. 1965 dec;12(120):1293–1305. Available from: <http://www.tandfonline.com/doi/abs/10.1080/14786436508228676>.
- [72] Li Y, Herbig M, Goto S, et al. Atomic scale characterization of white etching area and its adjacent matrix in a martensitic 100Cr6 bearing steel. *Materials Characterization*. 2017 jan;123:349–353. Available from: <http://linkinghub.elsevier.com/retrieve/pii/S1044580316311639><https://linkinghub.elsevier.com/retrieve/pii/S1044580316311639>
- [73] Beswick JM. Measurement of Carbon Levels in Structurally Transformed Sae 52100 Ball Bearing Steel By Microprobe Analysis. *Praktische Metallographie/Practical Metallography*. 1975;12(4):200–206.
- [74] Buchwald J, Heckel RW. An analysis of microstructural changes in 52100 steel bearings during cyclic stressing. *ASM Transactions Quarterly*. 1968;61:750–756.
- [75] Vegter RH, Slycke JT. Metal Physics and Rolling Contact Fatigue Testing. In: *Bearing steel technologies: 9th volume, advances in rolling contact fatigue strength testing and related substitute technologies*. 100 Barr Harbor Drive, PO Box C700, West Conshohocken, PA 19428-2959: ASTM International; 2012. p. 341–352. Available from: <http://www.astm.org/doiLink.cgi?STP104475>.
- [76] Cottrell AH, Bilby BA. Dislocation Theory of Yielding and Strain Ageing of Iron. *Proceedings of the Physical Society Section A*. 1949 jan;62(1):49–62. Available from: <http://stacks.iop.org/0370-1298/62/i=1/a=308?key=crossref.3c9382522ff3c88cc74532c2a4ee6cba>.
- [77] Kang JH, Hosseinkhani B, Rivera-Díaz-del Castillo PEJ. Rolling contact fatigue in bearings: multiscale overview. *Materials Science and Technology*. 2012 jan;28(1):44–49. Available from: <http://www.tandfonline.com/doi/full/10.1179/174328413X13758854832157>.
- [78] Hahn GT, Bhargava V, Chen Q. The cyclic stress-strain properties, hysteresis loop shape, and kinematic hardening of two high-strength bearing steels. *Metallurgical Transactions A*. 1990 feb;21(2):653–665. Available from: <http://link.springer.com/10.1007/BF02671936>.
- [79] Warhadpande A, Sadeghi F, Evans RD. Microstructural Alterations in Bearing Steels under Rolling Contact Fatigue: Part 2—Diffusion-Based Modeling Approach. *Tribology Transactions*. 2014 jan;57(1):66–76. Available from: <http://www.tandfonline.com/doi/abs/10.1080/10402004.2013.847999>.
- [80] Shewmon P. *Diffusion in Solids*. Cham: Springer International Publishing; 2016. Available from: <http://link.springer.com/10.1007/978-3-319-48206-4>
- [81] Warhadpande A, Sadeghi F, Kotzalas MN, et al. Effects of plasticity on subsurface initiated spalling in rolling contact fatigue. *International Journal of Fatigue*. 2012 mar;36(1):80–95. Available from: <http://dx.doi.org/10.1016/j.ijfatigue.2011.08.012><https://linkinghub.elsevier.com/retrieve/pii/S0142112311002222>
- [82] Serebrinsky S. A quantum-mechanically informed continuum model of hydrogen embrittlement. *Journal of the Mechanics and Physics of Solids*. 2004 oct;52(10):2403–2430. Available from: <https://linkinghub.elsevier.com/retrieve/pii/S0022509604000341>.
- [83] Dadfarnia M, Martin ML, Nagao A, et al. Modeling hydrogen transport by dislocations. *Journal of the Mechanics and Physics of Solids*. 2015 may;78:511–525. Available from: <http://dx.doi.org/10.1016/j.jmps.2015.03.002><https://linkinghub.elsevier.com/retrieve/pii/S0022509615000587>
- [84] Birnbaum H, Sofronis P. Hydrogen-enhanced localized plasticity—a mechanism for hydrogen-related fracture. *Materials Science and Engineering: A*. 1994;176(1-2):191–202.

- [85] Clouet E, Garruchet S, Nguyen H, et al. Dislocation interaction with C in  $\alpha$ -Fe: A comparison between atomic simulations and elasticity theory. *Acta Materialia*. 2008 aug; 56(14):3450–3460. Available from: <https://linkinghub.elsevier.com/retrieve/pii/S1359645408002218>
- [86] Laird C, Buchinger L. Hardening behavior in fatigue. *Metallurgical Transactions A*. 1985 dec;16(12):2201–2214. Available from: <http://link.springer.com/10.1007/BF02670419>
- [87] Mughrabi H. Dislocations in Fatigue. In: *Dislocations and properties of real materials: proceedings of the conference to celebrate the fiftieth anniversary of the concept of dislocation in crystals*; London. Institute of Metals; 1985. p. 244–262.
- [88] Neumann P. Low energy dislocation configurations: A possible key to the understanding of fatigue. *Materials Science and Engineering*. 1986 aug;81(C):465–475. Available from: <https://linkinghub.elsevier.com/retrieve/pii/0025541686902843>